Global Estimation of the Eddy Kinetic Energy Dissipation from a Diagnostic Energy Balance

Romain Torres[1], Robin Waldman[2], Julian Mak[3], and Roland Séférian[4]

[1]Météo-France
[2]Centre National de Recherches Météorologiques (CNRM), Météo France/CNRS
[3]HKUST
[4]CNRM (Météo-France/CNRS)

June 1, 2023

Abstract

Mesoscale eddies regulate the ocean heat and carbon budgets. However, how and where the kinetic energy flows out from the mesoscale reservoir remains uncertain. In this study, a simplified equation of the mesoscale energy budget is used to obtain a global estimation of the eddy dissipation rate. This framework is first validated in a global ocean model and then applied to a density climatology and a global reconstruction of the eddy kinetic energy field. We find a global disipation rate of 0.66±0.19 TW for the mesoscale kinetic energy, in agreement with recent independent estimates. The results also show an intense dissipation near western boundary currents and in the Antarctic Circumpolar Current, where both large levels of energy and baroclinic conversion occur. The resulting geographical distribution of the dissipation rate brings new insights for closing the ocean kinetic energy budget, as well as constraining future mesoscale parameterizations and associated mixing processes.

Global Estimation of the Eddy Kinetic Energy Dissipation from a Diagnostic Energy Balance

Romain Torres[1], Robin Waldman[1], Julian Mak[2,3], Roland Séférian[1]

[1]CNRM, Université de Toulouse, Météo-France, CNRS, Toulouse, France
[2]Department of Ocean Science, Hong Kong University of Science and Technology, Hong Kong
[3]Center for Ocean Research in Hong Kong and Macau, Hong Kong University of Science and Technology, Hong Kong

Key Points:

- Global mesoscale eddy kinetic energy dissipation rate estimated to 0.66 ± 0.19 TW from observation-based and statistically analysed datasets
- High dissipation of geostrophic eddies are found in the western boundary currents and the Antarctic Circumpolar Current
- Estimation of the eddy dissipation timescale from observations to inform future parameterization development

Corresponding author: Romain Torres, romain.torres@meteo.fr

Abstract

Mesoscale eddies regulate the ocean heat and carbon budgets. However, how and where the kinetic energy flows out from the mesoscale reservoir remains uncertain. In this study, a simplified equation of the mesoscale energy budget is used to obtain a global estimation of the eddy dissipation rate. The framework is first validated in a global ocean model and then applied to a density climatology and a global reconstruction of the eddy kinetic energy field. We find a global disipation rate of $0.66 \pm 0.19\,\mathrm{TW}$ for the mesoscale kinetic energy, in agreement with recent independent estimates. The results also show an intense dissipation near western boundary currents and in the Antarctic Circumpolar Current, where both large levels of energy and baroclinic conversion occur. The resulting geographical distribution of the dissipation rate brings new insights for closing the ocean kinetic energy budget, as well as constraining future mesoscale parameterizations and associated mixing processes.

Plain Language Summary

The ocean is home to abundant and large swirls from tens to hundreds of kilometers, called "mesoscale eddies". These eddies contain more momentum than most ocean currents and can thus impact the climate evolution. There are now good reasons to believe the effect of mesoscale eddies are directly related to their strength, and so to their kinetic energy. However, how the energy is removed from these eddies is still unclear mostly due to instrumental and theoretical limitations. In this work, a simplification of the eddy energetic behavior is used to indirectly estimate the dissipation from observations of temperature, salinity and surface currents. Our results confirm intensified dissipation near strong ocean currents and hence constitute a new attempt for the global reconstruction of the eddy kinetic energy dissipation in the world ocean. The work presented here is consistent and complementary to other studies and can help us to understand the ocean energy cycle.

1 Introduction

Oceans play a key role in setting transient climate change (Fox-Kemper et al., 2021), having absorbed the bulk of the excess energy due to anthropogenic emissions (von Schuckmann et al., 2020), redistributing heat across the Earth (Zanna et al., 2019) and affecting sea level rise (Couldrey et al., 2020). The oceans are also a leading component for the anthropogenic carbon uptake (Friedlingstein et al., 2022) and host a diversity of ecosystems and marine resources (Cooley et al., 2022).

Among the many dynamical processes present in the oceans, geostrophic or mesoscale eddies are central in the transport of tracers and can impact on large scale motions. Varying in size from kilometers to hundreds of kilometers, they dominate the oceanic kinetic energy reservoir (Ferrari & Wunsch, 2009) and significantly influence the transport and mixing of water masses in the ocean. While knowledge of the eddy energy field is essential for assessing these properties (Cessi, 2008; Fox-Kemper et al., 2019; Groeskamp et al., 2020), the mesoscale energetics are still not well understood. More precisely, the way the eddy energy dissipates and is transferred toward other scales is complex and poorly constrained by theories and observations. The dissipation of eddy kinetic energy is also associated to the ocean diapycnal mixing through different processes (Naveira Garabato et al., 2004; Saenko et al., 2012; Melet et al., 2015; Yang et al., 2019) and can in turn impact the global overtuning circulation (Saenko et al., 2018).

A variety of processes are able to dissipate or transfer the mesoscale mechanical energy. Among them, interactions of geostrophic flow with bottom topography either by direct dissipation drag (Sen et al., 2008; Arbic et al., 2009) and non-propagating form drag (Klymak, 2018; Klymak et al., 2021) or by scattering into lee waves (Nikurashin & Ferrari, 2011) appear to be an important sink of eddy energy. Other candidates include the forward cascade due to instabilities of unbalanced motions (Molemaker et al., 2010; Barkan et al., 2015), direct interactions with the internal wave field (Polzin, 2010) and suppression by wind work (Renault et al., 2019; Rai et al., 2021). The reader can refer to the review of McWilliams (2016) for a more comprehensive description of involved processes.

Observational estimates of energy dissipation in the ocean are extremely limited. If some global quantification exists, large uncertainties remain. The work of Sen et al. (2008) estimates from different observations a global dissipation rate by quadratic bottom boundary layer drag in the range of 0.2-0.8 TW. The large spread in the estimation is due to hypotheses in the calculation of the bottom geostrophic velocities. Regarding other processes, the lee waves generation rate from geostrophic motion is estimated between 0.2 TW and 0.49 TW (Nikurashin & Ferrari, 2011; Scott et al., 2011) while in a recent study, Rai et al. (2021) compute a global "eddy killing" rate from the wind of 0.05 TW at scales smaller than 260 km. Recently, sufficient amount of satellite altimeter data and efficient tracking algorithms have allowed oceanographers to characterize more systematically eddy properties (e.g. diameters, direction and lifetimes) both globally (Chelton et al., 2011) and regionally (Braby et al., 2016; Ji et al., 2018). However, only a few studies derive an overall map of eddy sinks from these Lagrangian analyses (Zhai et al., 2010; Xu et al., 2011; Sun et al., 2017).

The aim of this paper is to estimate a global dissipation rate of the mesoscale kinetic energy from observation-based climatology datasets. To do so, a simple diagnostic energy balance is used, leading to a relation where the eddy dissipation is directly related to the mean ocean stratification and proportional to the eddy kinetic energy. This relation is first introduced in section 2. Section 3 proposes a global reconstruction of the mesoscale eddy dissipation rate using satellite observations and available climatology of temperature and salinity. We finally discuss the hypotheses of this work in section 4, while section 5 summarizes the implications and the main conclusions.

2 A Simplified Mesoscale Energy Budget

We first derive a simplified mesoscale energy balance to retrieve an estimate of the eddy dissipation. Here we term "dissipation" the energy flux going out to the mesoscale reservoir although the energy is transferred to other scales, which in turn can provide a route to dissipation. We use the depth-integral energy budget introduced by the GEOMETRIC parameterization (Mak et al., 2018) applied to the eddy kinetic energy (EKE):

$$\frac{\partial}{\partial t}\int \mathrm{EKE}\,dz + \underbrace{\nabla_H \cdot \left(\widetilde{\mathbf{u}}^z \int \mathrm{EKE}\,dz\right)}_{\text{advection}} = \underbrace{\int \kappa_{gm}\frac{M^4}{N^2}\,dz}_{\text{production}} - \underbrace{\lambda\int \mathrm{EKE}\,dz}_{\text{dissipation}} + \underbrace{\eta_E \nabla_H^2 \int \mathrm{EKE}\,dz}_{\text{diffusion}}, \tag{1}$$

where the vertical integration is applied from the bottom to the surface. The depth-integrated eddy kinetic energy is here advected by the depth-averaged velocity $\widetilde{\mathbf{u}}^z$. The production term is assumed to be dominated by the baroclinic instability (Robinson & McWilliams, 1974) and represents the eddy growth resulting from isopycnal flattening. Consistent with the so-called Gent and McWilliams parameterization (Gent & McWilliams, 1990; Gent et al., 1995), it involves an eddy diffusivity coefficient κ_{gm} related to the horizontal and vertical buoyancy stratification, respectively M^2 and N^2, defined later in Equation 4. For simplicity, all the dissipative processes are approximated as a linear damping at a rate λ. Finally the eddy energy field is diffused horizontally with the last right hand side term modulated by a diffusivity η_E. In its original form, GEOMETRIC is a budget for the total (potential plus kinetic) eddy energy, but in the present study only the kinetic energy is considered since the baroclinic instability is the main source for the EKE reservoir (von Storch et al., 2012).

Marshall et al. (2012) have proposed a scaling for κ_{gm} where the coefficient is proportional to the total eddy energy. Again we adapt this framework by using the eddy kinetic energy only, consistent with the results from Bachman et al. (2017) who find modest differences when changing the type of energy in the scaling of κ_{gm}. Following the work of Mak et al. (2018), a two-dimensional formulation is used:

$$\kappa_{gm} = \alpha \, \frac{\int \mathrm{EKE} \, dz}{\int (M^2/N) \, dz}, \tag{2}$$

where α is a non-dimensional constant which represents the eddy efficiency to convert mean available potential energy into mesoscale kinetic energy.

We finally simplify the energy budget by assuming a diagnostic balance on decadal time scales between the baroclinic production and the linear dissipation terms (Marshall et al., 2017). Then, injecting the scaling of Equation 2 into the production term, both the source and dissipation terms are now proportional to the depth-integrated EKE. This leads to a diagnostic relation between the linear eddy dissipation coefficient λ and the ocean stratification:

$$\lambda = \alpha \, \frac{\int \left(M^4/N^2\right) dz}{\int \left(M^2/N\right) \, dz}. \tag{3}$$

Within this simple energy balance, the eddy dissipation coefficient is a function of the ocean large scale stratification and the eddy efficiency α only. In this study, we focus on the simple case where α has no time and spatial dependence and we choose $\alpha = 0.1$ deduced from previous studies (Marshall et al., 2012; Bachman et al., 2017; Mak et al., 2018; Poulsen et al., 2019; Wei et al., 2022; Mak, Marshall, et al., 2022). See section 4 for a discussion on the value of α.

In the work of Marshall et al. (2017) and Mak et al. (2017), a similar energy balance is considered (their Equations 6 and 20 respectively) but used for a different purpose in order to diagnose the emergent eddy saturation in idealized configurations. They employed circumpolar domains where the advection and the diffusion of EKE naturally vanish. In the following, a more local approach is used and the eddy energy balance in Equation 3 is considered regionally, at a typical scale of $\mathcal{O}(1000)\,\mathrm{km}$.

The eddy energy balance is first validated within a global ocean model (see Text S1 of the Supporting Information for details of the numerical configuration). To summarize, the stand-alone ocean simulation includes the GEOMETRIC parameterization (Mak, Marshall, et al., 2022) which discretizes the Equation 1. Monthly means of model outputs, including each EKE trends, are stored and used to evaluate the validity of the eddy energy balance. In accordance with the climatology used in section 3, the simulation outputs are analysed over the 23-year period from 1995 to 2017. We find a slight dominance of the dissipation term over the production, leading to a modest underestimation of the eddy dissipation coefficient λ. However, the proposed diagnostic eddy energy balance is overall valid when analysing the remaining terms of Equation 1 (see Figures S1 and S2 of the Supporting Information), allowing the use of a time-averaged stratification to compute the coefficient λ. Finally, we estimate a mean relative error of 35% on the coefficient λ, a figure used to compute the uncertainty range in our results (see error and uncertainty quantification in Text S1 of the Supporting Information).

3 Eddy Dissipation from global Observations

3.1 Datasets

Retrieving the eddy dissipation rate from Equation 3 only requires an averaged large-scale density field from which the ocean stratification can be computed. For that, we use the in-situ temperature and practical salinity reconstructions from the World Ocean Atlas 2018 (WOA18) climatology (Garcia et al., 2019) to compute the conservative temperature Θ, the absolute salinity S_A and the in-situ density ρ using the TEOS-10 equation of state (IOC et al., 2010) from the GSW python toolbox (Firing et al., 2021). Then, both horizontal and vertical stratifications M^2 and N^2 are computed as:

$$M^2 = \frac{g}{\rho_0}|\nabla_h \rho| \,, \quad N^2 = \frac{g}{\rho_0}\left(\alpha_\Theta \frac{\partial \Theta}{\partial z} - \beta_S \frac{\partial S_A}{\partial z}\right), \tag{4}$$

with g the gravity acceleration, $\rho_0 = 1026$ kg/m^3 a reference density, and α_Θ and β_S the seawater thermal expansion and saline contraction coefficients respectively. A relatively large time span climatological mean is needed as the balance Equation 3 is valid typically at the large-scale and over decadal timescales. We therefore use a merge of two WOA18 datasets covering a 23-year period from 1995 to 2017, which incorporates the global Argo float measurements from 2005.

An estimation of the EKE is required to deduce the final dissipation rate defined by the second right hand side term in Equation 1. Similar to the work of Groeskamp et al. (2020), we compute the surface eddy kinetic energy from sea surface geostrophic velocity anomalies (u_0', v_0') with respect to the 1995-2017 period and collected at 1/4° resolution from the European Union-Copernicus Marine Service (2021). The resulting EKE map is then regridded onto the WOA18 grid while ensuring energy conservation. Since a three-dimensional energy field is needed, we apply a vertical structure function assumed to be separable so that the eddy velocity components can be formulated as $(u',\, v') = \phi(z)(u_0',\, v_0')$. The structure function $\phi(z)$ assumes a rough bottom topography (LaCasce & Groeskamp, 2020) and is found by solving a differential equation throughout the water column (see calculation details in Text S2 of the Supporting Information). The function $\phi(z)$ represents the variation of the eddy velocity with depth and is used to compute the depth-integrated EKE:

$$\int \mathrm{EKE}\, dz = \int \frac{\left(u_0'^2 + v_0'^2\right)}{2} \phi(z)^2 \, dz. \tag{5}$$

3.2 The Eddy Dissipation Timescale

From the WOA18 dataset, both the horizontal and vertical stratifications are computed. The integral of these metrics over the whole depth is mapped in Figure 1a,b. The horizontal stratification turns out to be a good proxy for the shear found in strong oceanic baroclinic currents, notably western boundary currents and the Antarctic Circumpolar Current (ACC). To a lesser extent, it also shows the subtropical gyre signatures and their western intensification. We also note extreme and noisy values at high latitudes, especially in the Arctic Ocean, likely due to a lack of observations during winter in the WOA18 dataset. On the other hand, the vertical stratification map shows a general equatorward increase, with regionally reduced stratification over eastern boundary upwelling systems and increased stratification in the vicinity of major river mouths. On top of that, both parameters show a strong bathymetric dependence, as they are defined as vertical integrals.

These maps help to understand the horizontal distribution of the eddy dissipation timescale λ^{-1} (units in days) obtained from Equation 3 and shown in Figure 1c. Very short eddy timescales are found near the Gulf stream, the Kuroshio and the Agulhas regions as well as along the ACC. These geographical patterns were expected since they are also regions of strong baroclinic currents. The same is also true along the north Atlantic subpolar gyre. As already pointed out in the horizontal stratification map, the short dissipation timescales found at high latitudes in the Arctic ocean and off Antarctica are doubtful. This result, although partly explained by the extremely weak vertical stratification in these regions, lacks of in-situ measurement and should be used with caution. Conversely, the dissipation timescale is large at low latitudes, in the equatorial regions and in the interior of subtropical gyres. Both the reduced horizontal shear and the high vertical stratification can explain the long eddy timescales found at those locations. To a lesser extent, a similar pattern is found in the north Pacific subpolar gyre.

This estimate can be compared to the work of Mak, Avdis, et al. (2022) who constrain the same eddy dissipation timescale using a kinematic inverse calculation inferred from an eddy permitting ocean circulation model. Similarly, short timescales are found near the western boundary currents and the ACC while subtropical gyre signatures are absent from their spatial distribution. Nevertheless, they find long dissipation timescales in eastern boundary regions, a feature less marked in our global estimation. In addition, within our eddy energy balance the eddy dissipation timescale is comparable with (although not equivalent to) the baroclinic growth rate. For instance, the eddy growth rate computed through a linear analysis by Tulloch et al. (2011) retreives similar spatial patterns, even if the present work shows higher values at mid and low latitudes.

3.3 Eddy Kinetic Energy Reconstruction

From altimetry records, the surface eddy kinetic energy is computed and averaged between 1995 and 2017. The resulting map is shown in Figure 2a. The western boundary currents, their extension, the ACC as well as the equatorial band show strong signatures with high levels of energy. The Indian Ocean also displays significant surface EKE while very weak levels are found at high latitudes, in the Arctic and next to the Antarctic, but also in the interior of subtropical gyres. The map is comparable to previous estimates of eddy kinetic energy also based on altimetry (Martinez-Moreno et al., 2020; Groeskamp et al., 2020).

Figure 2b shows the vertically-integrated EKE deduced from Equation 5. The use of the baroclinic surface mode vertical function clearly intensifies the eddy activity in the Southern Ocean while weakening the energy patterns in the tropics and subtropics. The North Atlantic Current and the Labrador Sea also display deep vertical structures which in turn reinforce the integrated EKE near the Gulf Stream extension (see Figure S4 in the Supporting Information). In addition, the bathymetry affects the final map and more particularly, almost no energy is found near the coasts nor in shallow waters.

Integrated over the whole domain, the total EKE reservoir accounts for 4.42 EJ (10^{18}J). For comparison with other studies based on high resolution models, von Storch et al. (2012) found 3.55 EJ while the work of Yu and Metzger (2019) estimated a smaller EKE reservoir of 1.76 EJ. These results therefore give credit to our method and the use of the surface mode vertical structure in the reconstruction of the geostrophic eddy field.

3.4 Global Estimate of the Eddy Kinetic Energy Dissipation

By combining the estimated eddy dissipation timescale and the vertical integral EKE, the dissipation rate of mesoscale kinetic energy is obtained and mapped in Figure 3. To some extent, the map retains the horizontal patterns of the integrated EKE (Figure 2b), although intensified. Indeed, boundary currents and the ACC are found to be highly dissipative regions of mesoscale eddies since they hold large levels of energy while also presenting short eddy dissipation timescales (Figure 1c). In the northern hemisphere, intense EKE dissipation is found in the Kuroshio as well as the Gulf Stream region and its extension. In the southern hemisphere, the Agulhas Current and its retroflection, the Zapiola gyre and the ACC signatures are striking with an eddy dissipation rate often exceeding 25 mW/m^2.

Table 1: Domain-integrated dissipation rate of the eddy kinetic energy over oceanic basins displayed in Figure 3. The longitude and latitude bounds for each box are also indicated as well as the associated ocean area. The ACC basin is defined following the mask created by Martinez-Moreno et al. (2020) but modified to include a part of the Agulhas retroflection between 52–100°E and southward to 42°S, while removing the boxes used for the southern boundary current. The surface average represents the ratio between the integrated dissipation rate and the basin area.

	Global	Gulf Stream	Kuroshio	Agulhas	Brazil-Malvinas	ACC
Longitude	-	73°-39°W	140°-175°E	14°-52°E	59.5°-32°W	-
Latitude	-	33°-44°N	30°-42°N	30°-44°S	34.5°-50.5°S	-
Surface area (10^6 km^2)	344.3	3.5	4.1	4.7	4.1	66.6
% of total	(100 %)	(1.0 %)	(1.2 %)	(1.4 %)	(1.2 %)	(19.4 %)
Dissipation rate (TW)	0.66 ± 0.19	0.05 ± 0.01	0.03 ± 0.01	0.07 ± 0.02	0.03 ± 0.01	0.25 ± 0.04
% of total	(100 %)	(7.8 ± 2.7 %)	(4.5 ± 1.8 %)	(10.6 ± 3.9 %)	(5.0 ± 2.2 %)	(37.5 ± 12.8%)
Surface average (mW/m^2)	1.93 ± 0.56	14.82 ± 2.85	7.26 ± 2.02	14.97 ± 3.42	8.06 ± 2.64	3.34 ± 0.60

The map also reveals both the East Australian Current and the West Australian Current as places of mesoscale EKE dissipation. The latter is the only ocean eastern boundary upwelling region present on this global map.

Intermediate levels of EKE dissipation are found in the equatorial and subtropical bands, mostly in the Pacific Ocean. Even if these regions are theoretically less prone to baroclinic instability (Tulloch et al., 2011), the amount of computed EKE and the simple balance of Equation 3 produce a relatively large eddy dissipation. This pattern is not often observed in previous studies (Sen et al., 2008; Xu et al., 2011) but reflects the large number of attendent eddies in these regions (Chelton et al., 2011). Finally, the dissipation rate shows strong variations zonally with very weak EKE removal in the Eastern part of ocean basins. In particular the North and South Pacific subtropical gyres have a pronounced signature with a minimum of EKE dissipation found in the vicinity of the Alaska, the California and the Humboldt Currents. Both the horizontal distribution of EKE and of the dissipation timescale explain these patterns.

Since most of the mesoscale dissipation occurs in strong and deep-reaching currents, domain-integrated EKE dissipation rates are computed over the most energetic ocean regions and summarized in Table 1. Covering only a small part of the global ocean area, the four main western boundary current systems are responsible here for more than 25% of the total EKE sinks. It is particularly true in the Agulhas and the Gulf Stream regions with an average dissipation rate of 15 mW/m^2, one order of magnitude larger than the global average. The southern hemisphere clearly dominates the EKE dissipation with numerous dissipation hotspots, notably in the ACC which cumulates more than a third of the global dissipation.

In total, we find a global EKE dissipation rate of 0.66 ± 0.19 TW. This figure represents a substantial fraction of the $\sim$1 TW wind power input to the geostrophic field (Wunsch, 1998) and is close to the expected eddy potential to kinetic energy conversion rate (von Storch et al., 2012), confirming the key role of mesoscale eddies in the ocean energy cycle. Our results are also in the range of previous global estimations. Sen et al. (2008) computed an observed dissipation of geostrophic motion by bottom drag between 0.2 TW and 0.8 TW while Arbic et al. (2009) obtained a reduced range of 0.14-0.65 TW from different simulations. This finding suggests the bottom drag is a leading-order mechanism of mesoscale dissipation even if regional and cross-comparison studies are needed to better quantify the EKE dissipation processes.

4 Discussion

4.1 Validition of the Eddy Energy Balance

In section 2, a diagnostic eddy energy balance is presented where the energy sources by baroclinic instability are offset by a linear EKE dissipation. In this study, we use a coarse and global low-resolution model to verify this eddy energy balance. The simulation outputs tend to validate the framework but still indicate errors evaluated at 35%. These figures should be carefully interpreted since the model and the chosen parameterized energy budget necessarily present some biases. More precisely, the barotropic instability is neglected in Equation 1 although it could be a significant mechanism for the generation of mesoscale eddies (e.g. Gula et al., 2015; Maillard et al., 2022). However, at the global scale, model-based Lorenz energy cycle estimates suggest that baroclinic production by far exceeds its barotropic counterpart (von Storch et al., 2012). In addition, satellite observations have shown that eddies could efficiently propagate westward (Chelton et al., 2007, 2011; Zhai et al., 2010), indicating that advection may play a role in the EKE budget. Finally, recent studies indicate strong observed EKE variability (Ding et al., 2017; Martinez-Moreno et al., 2020) and possible long-term trends (Beech et al., 2022). Nonetheless, on the decadal time scale relatively small trends of EKE are found, supporting the hypothesis of a steady eddy kinetic energy reservoir. In order to account for all the aforementioned processes, eddy-rich and high-resolution models could be used to validate the eddy energy balance.

4.2 Sensitivity of the Eddy Dissipation to the Eddy Efficiency α

Another assumption in our method remains in the choice of the eddy efficiency α, and to our knowledge, there is no method to get an accurate estimation of this parameter in the global ocean. Bachman et al. (2017) use a suite of idealized channel simulations to compare several parameterizations of eddy transfer coefficients. They recommend the equilibrated long-term value of 0.2, even if the eddy efficiency takes different values during the eddy lifetime. Poulsen et al. (2019) diagnose the spatial structure of the eddy efficiency in the Southern Ocean with an eddy-resolving ocean circulation model. They recommend an average value as low as 0.043, consistent with the default value of 0.04 used in the GEOMETRIC parameterization (Mak et al., 2018; Mak, Marshall, et al., 2022). More recently, Wei et al. (2022) set the eddy efficiency to 0.07 in order to optimize their diagnostics of the eddy buoyancy fluxes in shelf and open ocean regions of eddy resolving simulations.

We also note that the eddy efficiency α in Equations 2 and 3 is different from the one introduced by Marshall et al. (2012) which use the total eddy energy instead of the EKE. However, the work of Bachman et al. (2017) suggests that switching the total to eddy kinetic energy in the scaling of κ_{gm} is physically consistent even if the coefficient should be increased by a given factor. Therefore, the above-mentioned values of the eddy efficiency should be increased when considering the EKE. Therefore we chose $\alpha = 0.1$ which is around twice the mean value diagnosed by Poulsen et al. (2019) in a realistic high-resolution model. Even if this value seems reasonable, we acknowledge the large uncertainties in our results due to the linear dependences of the EKE dissipation rate to α in the Equations 1 and 3. Indeed, taking extreme values of $\alpha = 0.04$ and $\alpha = 0.4$ would lead to a central estimate of 0.27 TW and 2.66 TW respectively, for the global EKE dissipation rate.

5 Conclusion

Dominating the ocean kinetic energy reservoir, mesoscale eddies are central to the Earth energy balance and transient climate response (Greatbatch et al., 2007; Chelton, 2013). Regarding the dissipation of this eddy kinetic energy (EKE), spatial distributions are still not well quantified in the global ocean. Indeed, direct and global measurements present serious instrumental difficulties making the problem of estimating the global eddy dissipation unsolved.

This present work proposes a global reconstruction of the EKE dissipation indirectly from observations. A simplified model for the ocean mesoscale energetics is employed, where baroclinic instability sources are perfectly balanced by sinks of EKE. In this model, the dissipative mechanisms are interpreted by means of eddy dissipation timescales and are directly related to the ocean stratification. The model and the energy balance were tested with an oceanic global circulation simulation using a parameterized eddy energy prognostic equation. In the whole ocean domain, the dissipation of EKE tends to approach its production by baroclinic instability, thereby confirming the adopted eddy energy balance. However, the dissipation also dominates some part of the ocean where other processes impact the EKE budget, illustrating the need for more realistic diagnostics of this eddy energy balance.

The framework is applied to available observations of temperature and salinity to compute a global map of the eddy dissipation timescale. The shortest timescales (higher dissipation) are found in the Southern Ocean and near strong western boundary currents coinciding with the regions prone to high baroclinic instability and large eddy growth rates (Tulloch et al., 2011). By projecting the eddy energy into depth using baroclinic surface modes (LaCasce & Groeskamp, 2020), a three-dimensional EKE field is also computed where the mean EKE reservoir is estimated to 4.42 EJ. Our work finally combines the two previous ingredients and provides a new global map for the EKE dissipation rate. Integrated over the whole ocean, the energy flux going out of the mesoscale reaches 0.66 ± 0.19 TW. Our study also confirms that most of the energy dissipation takes place in the southern hemisphere and more particularly in the Antarctic Circumpolar Current which accounts for 38% of the total dissipation. In addition, the main western boundary currents are found to be dissipation hotspots of EKE, accounting for more than 25% of the global dissipation.

Given the simplicity of the relation in Equation 3, the adopted framework allows an easy computation of the global EKE dissipation rate from indirect observations. Indeed, the method only requires a climatological mean field of density and surface geostrophic velocity anomalies, both of these being widely available observational data. Our results show important spatial patterns which if combined with other independent estimates, can help to understand the dissipation mechanisms. Since the dissipation of geostrophic kinetic energy remains one of the largest uncertainties in the ocean energy budget (Wunsch, 2004), it is thus crucial to quantify how and where the energy is removed from the EKE reservoir. Our results contribute to this goal and provide a new spatial distribution of the EKE dissipation rate in the world ocean.

Another important finding of this work is the estimation of the linear eddy dissipation coefficient λ employed in several ocean models (Cessi, 2008; Marshall & Adcroft, 2010; Mak et al., 2017, 2018). Recently, Mak, Marshall, et al. (2022) have demonstrated the sensitivity of global ocean circulation models using energy constrained mesoscale eddy parameterization to the eddy dissipation timescale λ^{-1}. In this study, we present the first estimate of the eddy timescale from global observation-based datasets. The resulting map can thus be used in eddy-parameterized ocean models to constrain the eddy energy dissipation and modulate the ocean stratification.

Open Research

This study has been conducted using E.U. Copernicus Marine Service Information: `https://doi.org/10.48670/moi-00148` for the altimetry dataset. Both climatology of temperature (Locarnini et al., 2018) and salinity (Zweng et al., 2018) from the World Ocean Atlas 2018 were downloaded through the National Oceanic and Atmospheric Administration website: `https://www.ncei.noaa.gov/archive/accession/NCEI-WOA18`, on 9 September

2022. Datas and Python scripts used to generate the results presented in this work are available on Zenodo : `https://sandbox.zenodo.org/record/1206326`.

Acknowledgments

This project has received support from the European Union's Horizon 2020 research and innovation programme under Grant Agreement N° 101003536 (ESM2025 – Earth System Models for the Future). JM also acknowledges support from both the RGC Early Career Scheme 2630020 and the Center for Ocean Research in Hong Kong and Macau, a joint research center between the Qingdao National Laboratory for Marine Science and Technology and Hong Kong University of Science and Technology. The authors would like to thank Sjoerd Groeskamp for his review and useful comments, and Jean-Baptiste Sallée for the discussions about observational measurements that make improvements in this final version of the article.

References

Arbic, B. K., Shriver, J. F., Hogan, P. J., Hurlburt, H. E., McClean, J. L., Metzger, E. J., ... Wallcraft, A. J. (2009, feb). Estimates of bottom flows and bottom boundary layer dissipation of the oceanic general circulation from global high-resolution models. *Journal of Geophysical Research*, *114*(C2). doi: 10.1029/2008jc005072

Bachman, S., Marshall, D., Maddison, J., & Mak, J. (2017). Evaluation of a scalar eddy transport coefficient based on geometric constraints. *Ocean Modelling*, *109*, 44–54. doi: 10.1016/j.ocemod.2016.12.004

Barkan, R., Winters, K. B., & Smith, S. G. L. (2015, jan). Energy cascades and loss of balance in a reentrant channel forced by wind stress and buoyancy fluxes. *Journal of Physical Oceanography*, *45*(1), 272–293. doi: 10.1175/JPO-D-14-0068.1

Beech, N., Rackow, T., Semmler, T., Danilov, S., Wang, Q., & Jung, T. (2022, sep). Long-term evolution of ocean eddy activity in a warming world. *Nature Climate Change*, *12*(10), 910–917. doi: 10.1038/s41558-022-01478-3

Braby, L., Backeberg, B. C., Ansorge, I., Roberts, M. J., Krug, M., & Reason, C. J. C. (2016, aug). Observed eddy dissipation in the Agulhas Current. *Geophysical Research Letters*, *43*(15), 8143–8150. doi: 10.1002/2016gl069480

Cessi, P. (2008, aug). An energy-constrained parameterization of eddy buoyancy flux. *Journal of Physical Oceanography*, *38*(8), 1807–1819. doi: 10.1175/2007JPO3812.1

Chelton, D. B. (2013, jul). Mesoscale eddy effects. *Nature Geoscience*, *6*(8), 594–595. doi: 10.1038/ngeo1906

Chelton, D. B., Schlax, M. G., & Samelson, R. M. (2011, oct). Global observations of nonlinear mesoscale eddies. *Progress in Oceanography*, *91*(2), 167–216. doi: 10.1016/j.pocean.2011.01.002

Chelton, D. B., Schlax, M. G., Samelson, R. M., & de Szoeke, R. A. (2007, aug). Global observations of large oceanic eddies. *Geophysical Research Letters*, *34*(15). doi: 10.1029/2007gl030812

Cooley, S., Schoeman, D., Bopp, L., Boyd, P., Donner, S., Ghebrehiwet, D., ... Skern-Mauritzen, M. (2022). Oceans and coastal ecosystems and their services. in: Climatechange 2022: Impacts, adaptation and vulnerability. contribution of working group ii to the sixth assessment report ofthe intergovernmental panel on climate change. In H.-O. Pörtner et al. (Eds.), (p. 379–550). Cambridge University Press, Cambridge,UK and New York, NY, USA. Retrieved from `https://www.ipcc.ch/report/ar6/wg2/downloads/report`

Couldrey, M. P., Gregory, J. M., Dias, F. B., Dobrohotoff, P., Domingues, C. M., Garuba, O., ... Zanna, L. (2020, oct). What causes the spread of model projections of ocean dynamic sea-level change in response to greenhouse gas forcing? *Climate Dynamics*, *56*(1-2), 155–187. doi: 10.1007/s00382-020-05471-4

Ding, M., Lin, P., Liu, H., & Chai, F. (2017, dec). Increased eddy activity in the northeastern Pacific during 1993–2011. *Journal of Climate*, *31*(1), 387–399. doi: 10.1175/jcli-d-17-0309.1

European Union-Copernicus Marine Service. (2021). *Global ocean gridded l4 sea surface heights and derived variables reprocessed (1993-ongoing).* Mercator Ocean International. doi: 10.48670/MOI-00148

Ferrari, R., & Wunsch, C. (2009, jan). Ocean circulation kinetic energy: Reservoirs, sources, and sinks. *Annual Review of Fluid Mechanics*, *41*(1), 253–282. doi: http://dx.doi.org/10.1146/annurev.fluid.40.111406.102139

Firing, E., , Filipe, Barna, A., & Abernathey, R. (2021). *Teos-10/gsw-python: v3.4.1.* Zenodo. Retrieved from `https://teos-10.github.io/GSW-Python/` doi: 10.5281/ZENODO.4631364

Fox-Kemper, B., Adcroft, A., Böning, C. W., Chassignet, E. P., Curchitser, E., Danabasoglu, G., ... Yeager, S. G. (2019, feb). Challenges and prospects in ocean circulation models. *Frontiers in Marine Science*, *6*. doi: 10.3389/fmars.2019.00065

Fox-Kemper, B., Hewitt, H., Xiao, C., Adalgeirsdóttir, G., Drijfhout, S., Edwards, T., ... Yu, Y. (2021). Ocean, cryosphere and sea level change. in climate change 2021: The physical science basis. contribution of working group i to the sixth assessment report of the intergovernmental panel on climate change. In M.-D. V. et al. (Eds.), (p. 1211–1362). Cambridge University Press,Cambridge, United Kingdom and New York, NY, USA. Retrieved from `https://www.ipcc.ch/report/ar6/wg1/chapter/chapter-9/`

Friedlingstein, P., Jones, M. W., O'Sullivan, M., Andrew, R. M., Bakker, D. C. E., Hauck, J., ... Zeng, J. (2022, apr). Global carbon budget 2021. *Earth System Science Data*, *14*(4), 1917–2005. doi: 10.5194/essd-14-1917-2022

Garcia, H. E., Boyer, T. P., Baranova, O. K., Locarnini, R. A., Mishonov, A. V., Grodsky, A., ... Zweng, M. M. (2019). World Ocean Atlas 2018: Product documentation. *NOAA National Centers for Environmental Information*. Retrieved from `https://www.ncei.noaa.gov/archive/accession/NCEI-WOA18`

Gent, P. R., & McWilliams, J. C. (1990, jan). Isopycnal mixing in ocean circulation models. *Journal of Physical Oceanography*, *20*(1), 150-155. doi: 10.1175/1520-0485(1990)020⟨0150:imiocm⟩2.0.co;2

Gent, P. R., Willebrand, J., McDougall, T. J., & McWilliams, J. C. (1995, apr). Parameterizing eddy-induced tracer transports in ocean circulation models. *Journal of Physical Oceanography*, *25*(4), 463–474. doi: 10.1175/1520-0485(1995)025⟨0463:peitti⟩2.0.co;2

Greatbatch, R. J., Zhai, X., Eden, C., & Olbers, D. (2007, apr). The possible role in the ocean heat budget of eddy-induced mixing due to air-sea interaction. *Geophysical Research Letters*, *34*(7). doi: 10.1029/2007gl029533

Groeskamp, S., LaCasce, J. H., McDougall, T. J., & Rogé, M. (2020, sep). Full-depth global estimates of ocean mesoscale eddy mixing from observations and theory. *Geophysical Research Letters*, *47*(18). Retrieved from `https://doi.org/10.1029/2020GL089425` doi: 10.1029/2020gl089425

Gula, J., Molemaker, M. J., & McWilliams, J. C. (2015, mar). Gulf Stream dynamics along the southeastern U.S. seaboard. *Journal of Physical Oceanography*, *45*(3), 690–715. doi: 10.1175/jpo-d-14-0154.1

IOC, SCOR, & IAPSO. (2010). The international thermodynamic equation of seawater – 2010: Calculation and use of thermodynamic properties. In (p. 196). UNESCO (English).

Ji, J., Dong, C., Zhang, B., Liu, Y., Zou, B., King, G. P., ... Chen, D. (2018, nov). Oceanic eddy characteristics and generation mechanisms in the Kuroshio extension region. *Journal of Geophysical Research: Oceans*, *123*(11), 8548–8567. doi: 10.1029/2018jc014196

Klymak, J. M. (2018, oct). Nonpropagating form drag and turbulence due to stratified flow over large-scale abyssal hill topography. *Journal of Physical Oceanography*, *48*(10), 2383–2395. doi: 10.1175/jpo-d-17-0225.1

Klymak, J. M., Balwada, D., Garabato, A. N., & Abernathey, R. (2021, may). Parameterizing nonpropagating form drag over rough bathymetry. *Journal of Physical Oceanography*, *51*(5), 1489–1501. doi: 10.1175/jpo-d-20-0112.1

LaCasce, J. H., & Groeskamp, S. (2020, oct). Baroclinic modes over rough bathymetry and the surface deformation radius. *Journal of Physical Oceanography*, *50*(10), 2835–2847. doi: 10.1175/jpo-d-20-0055.1

Locarnini, R. A., Mishonov, A. V., Baranova, O. K., Boyer, T. P., Zweng, M. M., García, H. E., ... Smolyar, I. (2018). World Ocean Atlas 2018, Volume 1: Temperature. *NOAA Atlas NESDIS*(81), 52.

Maillard, L., Boucharel, J., & Renault, L. (2022, aug). Direct and rectified effects of tropical instability waves on the eastern tropical Pacific mean state in a regional ocean model. *Journal of Physical Oceanography*, *52*(8), 1817–1834. doi: 10.1175/jpo-d-21-0300.1

Mak, J., Avdis, A., David, T., Lee, H. S., Na, Y., Wang, Y., & Yan, F. E. (2022). On constraining the mesoscale eddy energy dissipation time-scale. *Journal of Advances in Modeling Earth Systems*. doi: https://doi.org/10.1029/2022MS003223

Mak, J., Maddison, J. R., Marshall, D. P., & Munday, D. R. (2018, oct). Implementation of a geometrically informed and energetically constrained mesoscale eddy parameterization in an ocean circulation model. *Journal of Physical Oceanography*, *48*(10), 2363–2382. doi: 10.1175/jpo-d-18-0017.1

Mak, J., Marshall, D., Maddison, J., & Bachman, S. (2017, apr). Emergent eddy saturation from an energy constrained eddy parameterisation. *Ocean Modelling*, *112*, 125–138. doi: http://dx.doi.org/10.1016/j.ocemod.2017.02.007

Mak, J., Marshall, D. P., Madec, G., & Maddison, J. R. (2022, apr). Acute sensitivity of global ocean circulation and heat content to eddy energy dissipation timescale. *Geophysical Research Letters*, *49*(8). doi: 10.1029/2021GL097259

Marshall, D. P., & Adcroft, A. J. (2010, jan). Parameterization of ocean eddies: Potential vorticity mixing, energetics and Arnold's first stability theorem. *Ocean Modelling*, *32*(3-4), 188–204. doi: 10.1016/j.ocemod.2010.02.001

Marshall, D. P., Ambaum, M. H. P., Maddison, J. R., Munday, D. R., & Novak, L. (2017, jan). Eddy saturation and frictional control of the Antarctic Circumpolar Current. *Geophysical Research Letters*, *44*(1), 286–292. doi: 10.1002/2016gl071702

Marshall, D. P., Maddison, J. R., & Berloff, P. S. (2012, apr). A framework for parameterizing eddy potential vorticity fluxes. *Journal of Physical Oceanography*, *42*(4), 539–557. doi: 10.1175/jpo-d-11-048.1

Martinez-Moreno, J., Hogg, A., England, M., Constantinou, N. C., Kiss, A. E., & Morrison, A. (2020, oct). Global changes in oceanic mesoscale currents over the satellite altimetry record.
doi: 10.21203/rs.3.rs-88932/v1

McWilliams, J. C. (2016, may). Submesoscale currents in the ocean. *Proceedings of the Royal Society A: Mathematical, Physical and Engineering Sciences*, *472*(2189), 20160117. doi: 10.1098/rspa.2016.0117

Melet, A., Hallberg, R., Adcroft, A., Nikurashin, M., & Legg, S. (2015, mar). Energy flux into internal lee waves: Sensitivity to future climate changes using linear theory and a climate model. *Journal of Climate*, *28*(6), 2365–2384. doi: 10.1175/jcli-d-14-00432.1

Molemaker, M. J., McWilliams, J. C., & Capet, X. (2010, jun). Balanced and unbalanced routes to dissipation in an equilibrated Eady flow. *Journal of Fluid Mechanics*, *654*, 35–63. doi: 10.1017/S0022112009993272

Naveira Garabato, A. C., Polzin, K. L., King, B. A., Heywood, K. J., & Visbeck, M. (2004, jan). Widespread intense turbulent mixing in the southern ocean. *Science*, *303*(5655), 210–213. doi: 10.1126/science.1090929

Nikurashin, M., & Ferrari, R. (2011, apr). Global energy conversion rate from geostrophic flows into internal lee waves in the deep ocean. *Geophysical Research Letters*, *38*(8). doi: 10.1029/2011GL046576

Polzin, K. L. (2010, apr). Mesoscale eddy–internal wave coupling. part II: Energetics and results from PolyMode. *Journal of Physical Oceanography*, *40*(4), 789–801. doi:

10.1175/2009jpo4039.1

Poulsen, M. B., Jochum, M., Maddison, J. R., Marshall, D. P., & Nuterman, R. (2019). A geometric interpretation of southern ocean eddy form stress. *Journal of Physical Oceanography*, *49*(10), 2553–2570. doi: 10.1175/JPO-D-18-0220.1

Rai, S., Hecht, M., Maltrud, M., & Aluie, H. (2021, jul). Scale of oceanic eddy killing by wind from global satellite observations. *Science Advances*, *7*(28). doi: 10.1126/sciadv.abf4920

Renault, L., Marchesiello, P., Masson, S., & McWilliams, J. C. (2019, mar). Remarkable control of western boundary currents by *eddy killing*, a mechanical air-sea coupling process. *Geophysical Research Letters*, *46*(5), 2743–2751. doi: 10.1029/2018gl081211

Robinson, A. R., & McWilliams, J. C. (1974, jul). The baroclinic instability of the open ocean. *Journal of Physical Oceanography*, *4*(3), 281–294. doi: 10.1175/1520-0485(1974)004⟨0281:TBIOTO⟩2.0.CO;2

Saenko, O. A., Yang, D., & Gregory, J. M. (2018, oct). Impact of mesoscale eddy transfer on heat uptake in an eddy-parameterizing ocean model. *Journal of Climate*, *31*(20), 8589–8606. doi: 10.1175/jcli-d-18-0186.1

Saenko, O. A., Zhai, X., Merryfield, W. J., & Lee, W. G. (2012, apr). The combined effect of tidally and eddy-driven diapycnal mixing on the large-scale ocean circulation. *Journal of Physical Oceanography*, *42*(4), 526–538. doi: 10.1175/jpo-d-11-0122.1

Scott, R. B., Goff, J. A., Garabato, A. C. N., & Nurser, A. J. G. (2011, sep). Global rate and spectral characteristics of internal gravity wave generation by geostrophic flow over topography. *Journal of Geophysical Research*, *116*(C9). doi: 10.1029/2011jc007005

Sen, A., Scott, R. B., & Arbic, B. K. (2008, may). Global energy dissipation rate of deep-ocean low-frequency flows by quadratic bottom boundary layer drag: Computations from current-meter data. *Geophysical Research Letters*, *35*(9). doi: 10.1029/2008GL033407

Sun, M., Tian, F., Liu, Y., & Chen, G. (2017, feb). An improved automatic algorithm for global eddy tracking using satellite altimeter data. *Remote Sensing*, *9*(3), 206. doi: 10.3390/rs9030206

Tulloch, R., Marshall, J., Hill, C., & Smith, K. S. (2011, jun). Scales, growth rates, and spectral fluxes of baroclinic instability in the ocean. *Journal of Physical Oceanography*, *41*(6), 1057–1076. doi: 10.1175/2011jpo4404.1

von Schuckmann, K., Cheng, L., Palmer, M. D., Hansen, J., Tassone, C., Aich, V., … Wijffels, S. E. (2020, sep). Heat stored in the earth system: where does the energy go? *Earth System Science Data*, *12*(3), 2013–2041. doi: 10.5194/essd-12-2013-2020

von Storch, J.-S., Eden, C., Fast, I., Haak, H., Hernández-Deckers, D., Maier-Reimer, E., … Stammer, D. (2012, dec). An estimate of the Lorenz energy cycle for the world ocean based on the STORM/NCEP simulation. *Journal of Physical Oceanography*, *42*(12), 2185–2205. doi: https://doi.org/10.1175/JPO-D-12-079.1

Wei, H., Wang, Y., Stewart, A. L., & Mak, J. (2022, dec). Scalings for eddy buoyancy fluxes across prograde shelf/slope fronts. *Journal of Advances in Modeling Earth Systems*, *14*(12). doi: 10.1029/2022ms003229

Wunsch, C. (1998, nov). The work done by the wind on the oceanic general circulation. *Journal of Physical Oceanography*, *28*(11), 2332–2340. doi: 10.1175/1520-0485(1998)028⟨2332:twdbtw⟩2.0.co;2

Wunsch, C. (2004, jan). Vertical mixing, energy, and the general circulation of the oceans. *Annual Review of Fluid Mechanics*, *36*(1), 281–314. doi: 10.1146/annurev.fluid.36.050802.122121

Xu, C., Shang, X.-D., & Huang, R. X. (2011, feb). Estimate of eddy energy generation/dissipation rate in the world ocean from altimetry data. *Ocean Dynamics*, *61*(4), 525–541. doi: 10.1007/s10236-011-0377-8

Yang, Q., Nikurashin, M., Sasaki, H., Sun, H., & Tian, J. (2019, jan). Dissipation of mesoscale eddies and its contribution to mixing in the northern South China Sea. *Scientific Reports*, *9*(1). doi: 10.1038/s41598-018-36610-x

Yu, Z., & Metzger, E. J. (2019, jul). The impact of ocean surface currents on global eddy kinetic energy via the wind stress formulation. *Ocean Modelling*, *139*, 101399. doi: 10.1016/j.ocemod.2019.05.003

Zanna, L., Khatiwala, S., Gregory, J. M., Ison, J., & Heimbach, P. (2019, jan). Global reconstruction of historical ocean heat storage and transport. *Proceedings of the National Academy of Sciences*, *116*(4), 1126–1131. doi: 10.1073/pnas.1808838115

Zhai, X., Johnson, H. L., & Marshall, D. P. (2010, aug). Significant sink of ocean-eddy energy near western boundaries. *Nature Geoscience*, *3*(9), 608–612. doi: https://doi.org/10.1038/ngeo943

Zweng, M. M., Reagan, J. R., Seidov, D., Boyer, T. P., Locarnini, R. A., García, H. E., ... Smolyar, I. (2018). World Ocean Atlas 2018, Volume 2: Salinity. *NOAA Atlas NESDIS*(82), 50.

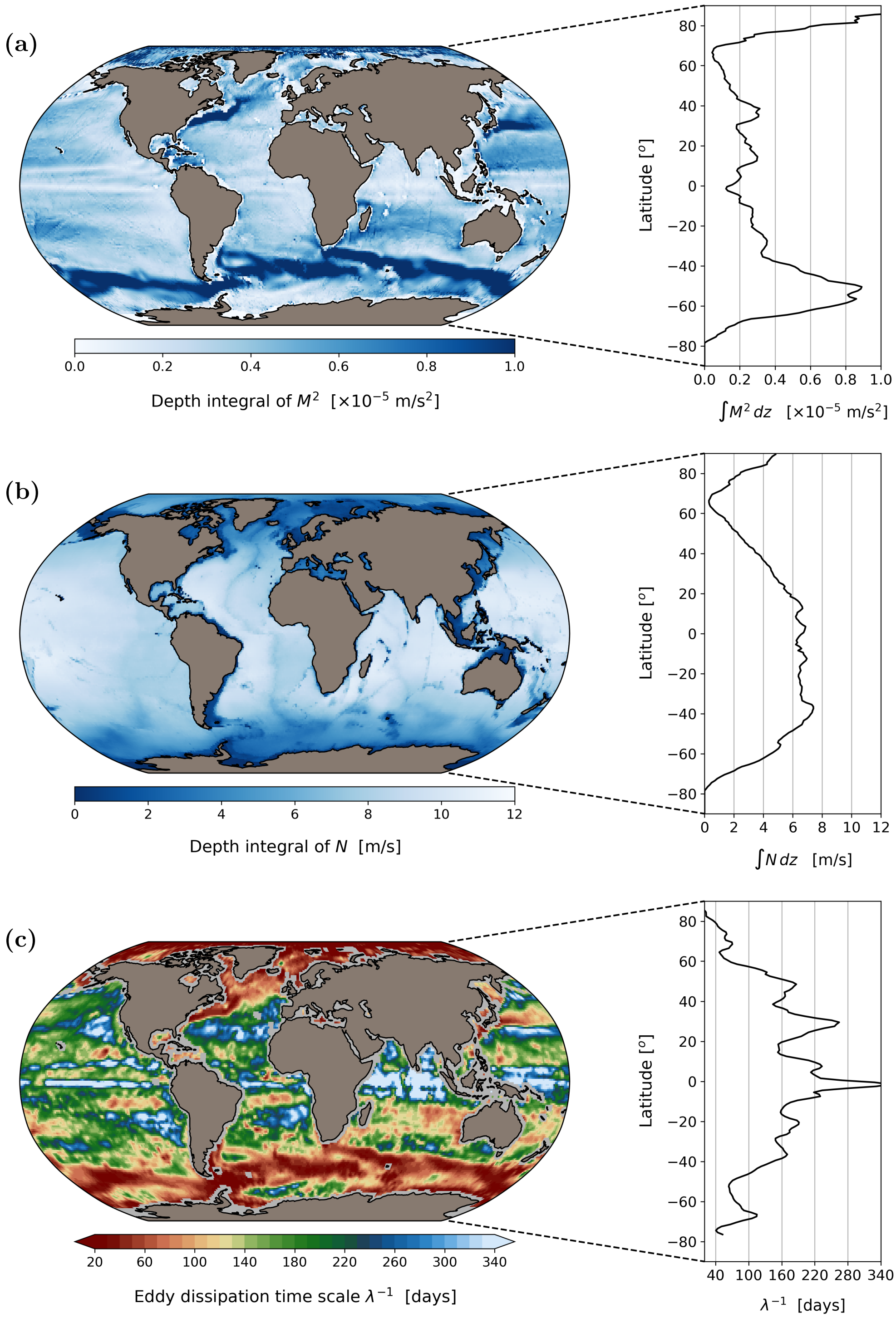

Figure 1: Depth integrals of (a) the horizontal buoyancy stratification M^2 (m/s^2) and (b) the Brunt-Väisälä frequency N (m/s) from the WOA18 climatology (Garcia et al., 2019). Equation 3 is used to compute (c) the global map of the eddy dissipation timescale λ^{-1} involving the ratio M^2/N while zonal averages are plotted on the right. In (a, b), the colormap is chosen so that dark blue leads to an increase of the eddy dissipation coefficient λ and conversely for light blue. In (c), we use a two-dimensional shapiro filter to reduce spatial noise.

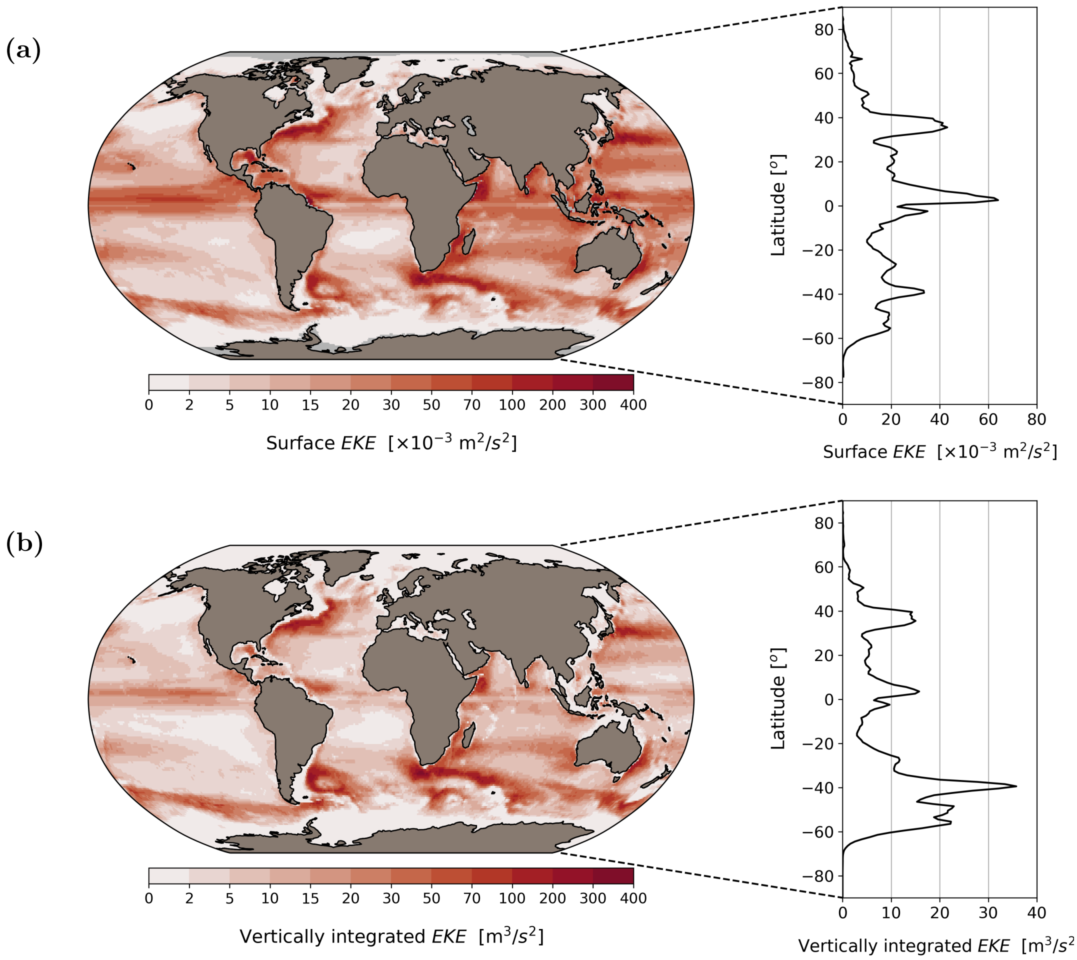

Figure 2: (a) Surface eddy kinetic energy (EKE) in m^2/s^2 deduced from the gridded altimetry (European Union-Copernicus Marine Service, 2021) and averaged over the period 1995–2017. (b) Vertically integrated EKE in m^3/s^2 deduced from the vertical structure function $\phi(z)$ in Equation 5. Both colorbars are chosen to illustrate the impact of $\phi(z)$ when computing the depth integral of EKE.

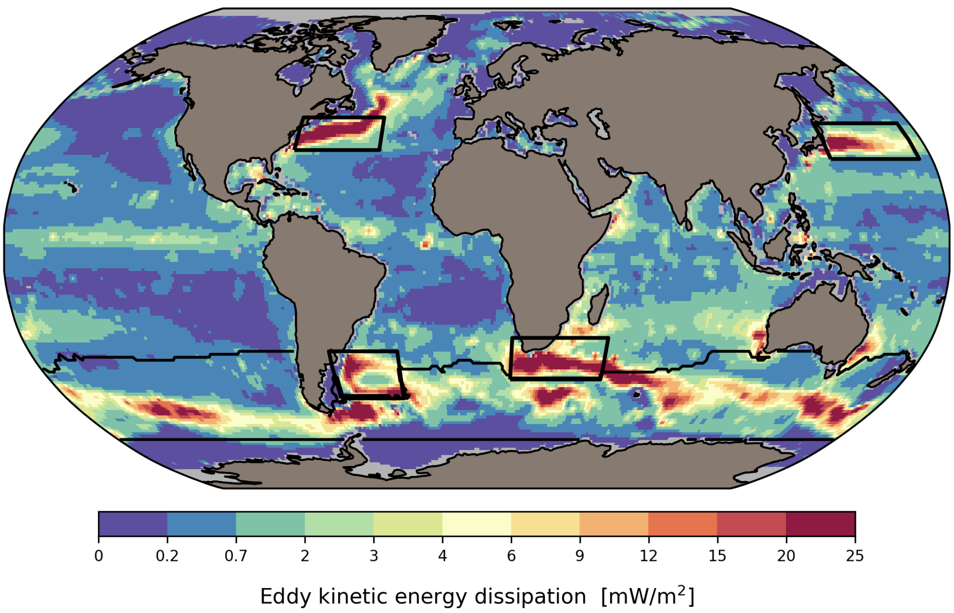

Figure 3: Vertically-integrated eddy dissipation rate in mW/m^2 estimated from the WOA18 climatology (Garcia et al., 2019) and the gridded altimetry (European Union-Copernicus Marine Service, 2021) over the period 1995–2017, with the use of the diagnostic relation in Equation 3. A reference density $\rho_0 = 1026$ kg/m^3 is used and the black boxes refer to the ocean basins defined in Table 1.

Global Estimation of the Eddy Kinetic Energy Dissipation from a Diagnostic Energy Balance

Romain Torres[1], Robin Waldman[1], Julian Mak[2,3], Roland Séférian[1]

[1]CNRM, Université de Toulouse, Météo-France, CNRS, Toulouse, France
[2]Department of Ocean Science, Hong Kong University of Science and Technology, Hong Kong
[3]Center for Ocean Research in Hong Kong and Macau, Hong Kong University of Science and Technology, Hong Kong

Key Points:

- Global mesoscale eddy kinetic energy dissipation rate estimated to 0.66 ± 0.19 TW from observation-based and statistically analysed datasets
- High dissipation of geostrophic eddies are found in the western boundary currents and the Antarctic Circumpolar Current
- Estimation of the eddy dissipation timescale from observations to inform future parameterization development

Corresponding author: Romain Torres, `romain.torres@meteo.fr`

Abstract

Mesoscale eddies regulate the ocean heat and carbon budgets. However, how and where the kinetic energy flows out from the mesoscale reservoir remains uncertain. In this study, a simplified equation of the mesoscale energy budget is used to obtain a global estimation of the eddy dissipation rate. The framework is first validated in a global ocean model and then applied to a density climatology and a global reconstruction of the eddy kinetic energy field. We find a global disipation rate of 0.66 ± 0.19 TW for the mesoscale kinetic energy, in agreement with recent independent estimates. The results also show an intense dissipation near western boundary currents and in the Antarctic Circumpolar Current, where both large levels of energy and baroclinic conversion occur. The resulting geographical distribution of the dissipation rate brings new insights for closing the ocean kinetic energy budget, as well as constraining future mesoscale parameterizations and associated mixing processes.

Plain Language Summary

The ocean is home to abundant and large swirls from tens to hundreds of kilometers, called "mesoscale eddies". These eddies contain more momentum than most ocean currents and can thus impact the climate evolution. There are now good reasons to believe the effect of mesoscale eddies are directly related to their strength, and so to their kinetic energy. However, how the energy is removed from these eddies is still unclear mostly due to instrumental and theoretical limitations. In this work, a simplification of the eddy energetic behavior is used to indirectly estimate the dissipation from observations of temperature, salinity and surface currents. Our results confirm intensified dissipation near strong ocean currents and hence constitute a new attempt for the global reconstruction of the eddy kinetic energy dissipation in the world ocean. The work presented here is consistent and complementary to other studies and can help us to understand the ocean energy cycle.

1 Introduction

Oceans play a key role in setting transient climate change (Fox-Kemper et al., 2021), having absorbed the bulk of the excess energy due to anthropogenic emissions (von Schuckmann et al., 2020), redistributing heat across the Earth (Zanna et al., 2019) and affecting sea level rise (Couldrey et al., 2020). The oceans are also a leading component for the anthropogenic carbon uptake (Friedlingstein et al., 2022) and host a diversity of ecosystems and marine resources (Cooley et al., 2022).

Among the many dynamical processes present in the oceans, geostrophic or mesoscale eddies are central in the transport of tracers and can impact on large scale motions. Varying in size from kilometers to hundreds of kilometers, they dominate the oceanic kinetic energy reservoir (Ferrari & Wunsch, 2009) and significantly influence the transport and mixing of water masses in the ocean. While knowledge of the eddy energy field is essential for assessing these properties (Cessi, 2008; Fox-Kemper et al., 2019; Groeskamp et al., 2020), the mesoscale energetics are still not well understood. More precisely, the way the eddy energy dissipates and is transferred toward other scales is complex and poorly constrained by theories and observations. The dissipation of eddy kinetic energy is also associated to the ocean diapycnal mixing through different processes (Naveira Garabato et al., 2004; Saenko et al., 2012; Melet et al., 2015; Yang et al., 2019) and can in turn impact the global overtuning circulation (Saenko et al., 2018).

A variety of processes are able to dissipate or transfer the mesoscale mechanical energy. Among them, interactions of geostrophic flow with bottom topography either by direct dissipation drag (Sen et al., 2008; Arbic et al., 2009) and non-propagating form drag (Klymak, 2018; Klymak et al., 2021) or by scattering into lee waves (Nikurashin & Ferrari, 2011) appear to be an important sink of eddy energy. Other candidates include the forward cascade due to instabilities of unbalanced motions (Molemaker et al., 2010; Barkan et al., 2015), direct interactions with the internal wave field (Polzin, 2010) and suppression by wind work (Renault et al., 2019; Rai et al., 2021). The reader can refer to the review of McWilliams (2016) for a more comprehensive description of involved processes.

Observational estimates of energy dissipation in the ocean are extremely limited. If some global quantification exists, large uncertainties remain. The work of Sen et al. (2008) estimates from different observations a global dissipation rate by quadratic bottom boundary layer drag in the range of 0.2-0.8 TW. The large spread in the estimation is due to hypotheses in the calculation of the bottom geostrophic velocities. Regarding other processes, the lee waves generation rate from geostrophic motion is estimated between 0.2 TW and 0.49 TW (Nikurashin & Ferrari, 2011; Scott et al., 2011) while in a recent study, Rai et al. (2021) compute a global "eddy killing" rate from the wind of 0.05 TW at scales smaller than 260 km. Recently, sufficient amount of satellite altimeter data and efficient tracking algorithms have allowed oceanographers to characterize more systematically eddy properties (e.g. diameters, direction and lifetimes) both globally (Chelton et al., 2011) and regionally (Braby et al., 2016; Ji et al., 2018). However, only a few studies derive an overall map of eddy sinks from these Lagrangian analyses (Zhai et al., 2010; Xu et al., 2011; Sun et al., 2017).

The aim of this paper is to estimate a global dissipation rate of the mesoscale kinetic energy from observation-based climatology datasets. To do so, a simple diagnostic energy balance is used, leading to a relation where the eddy dissipation is directly related to the mean ocean stratification and proportional to the eddy kinetic energy. This relation is first introduced in section 2. Section 3 proposes a global reconstruction of the mesoscale eddy dissipation rate using satellite observations and available climatology of temperature and salinity. We finally discuss the hypotheses of this work in section 4, while section 5 summarizes the implications and the main conclusions.

2 A Simplified Mesoscale Energy Budget

We first derive a simplified mesoscale energy balance to retrieve an estimate of the eddy dissipation. Here we term "dissipation" the energy flux going out to the mesoscale reservoir although the energy is transferred to other scales, which in turn can provide a route to dissipation. We use the depth-integral energy budget introduced by the GEOMETRIC parameterization (Mak et al., 2018) applied to the eddy kinetic energy (EKE):

$$\frac{\partial}{\partial t}\int \mathrm{EKE}\; dz + \underbrace{\nabla_H \cdot \left(\widetilde{\mathbf{u}}^z \int \mathrm{EKE}\; dz\right)}_{\text{advection}} = \underbrace{\int \kappa_{gm}\frac{M^4}{N^2}\; dz}_{\text{production}} - \underbrace{\lambda \int \mathrm{EKE}\; dz}_{\text{dissipation}} + \underbrace{\eta_E \nabla_H^2 \int \mathrm{EKE}\; dz}_{\text{diffusion}}, \tag{1}$$

where the vertical integration is applied from the bottom to the surface. The depth-integrated eddy kinetic energy is here advected by the depth-averaged velocity $\widetilde{\mathbf{u}}^z$. The production term is assumed to be dominated by the baroclinic instability (Robinson & McWilliams, 1974) and represents the eddy growth resulting from isopycnal flattening. Consistent with the so-called Gent and McWilliams parameterization (Gent & McWilliams, 1990; Gent et al., 1995), it involves an eddy diffusivity coefficient κ_{gm} related to the horizontal and vertical buoyancy stratification, respectively M^2 and N^2, defined later in Equation 4. For simplicity, all the dissipative processes are approximated as a linear damping at a rate λ. Finally the eddy energy field is diffused horizontally with the last right hand side term modulated by a diffusivity η_E. In its original form, GEOMETRIC is a budget for the total (potential plus kinetic) eddy energy, but in the present study only the kinetic energy is considered since the baroclinic instability is the main source for the EKE reservoir (von Storch et al., 2012).

Marshall et al. (2012) have proposed a scaling for κ_{gm} where the coefficient is proportional to the total eddy energy. Again we adapt this framework by using the eddy kinetic energy only, consistent with the results from Bachman et al. (2017) who find modest differences when changing the type of energy in the scaling of κ_{gm}. Following the work of Mak et al. (2018), a two-dimensional formulation is used:

$$\kappa_{gm} = \alpha \, \frac{\int \mathrm{EKE} \, dz}{\int (M^2/N) \, dz}, \tag{2}$$

where α is a non-dimensional constant which represents the eddy efficiency to convert mean available potential energy into mesoscale kinetic energy.

We finally simplify the energy budget by assuming a diagnostic balance on decadal time scales between the baroclinic production and the linear dissipation terms (Marshall et al., 2017). Then, injecting the scaling of Equation 2 into the production term, both the source and dissipation terms are now proportional to the depth-integrated EKE. This leads to a diagnostic relation between the linear eddy dissipation coefficient λ and the ocean stratification:

$$\lambda = \alpha \, \frac{\int \left(M^4/N^2\right) dz}{\int \left(M^2/N\right) \, dz}. \tag{3}$$

Within this simple energy balance, the eddy dissipation coefficient is a function of the ocean large scale stratification and the eddy efficiency α only. In this study, we focus on the simple case where α has no time and spatial dependence and we choose $\alpha = 0.1$ deduced from previous studies (Marshall et al., 2012; Bachman et al., 2017; Mak et al., 2018; Poulsen et al., 2019; Wei et al., 2022; Mak, Marshall, et al., 2022). See section 4 for a discussion on the value of α.

In the work of Marshall et al. (2017) and Mak et al. (2017), a similar energy balance is considered (their Equations 6 and 20 respectively) but used for a different purpose in order to diagnose the emergent eddy saturation in idealized configurations. They employed circumpolar domains where the advection and the diffusion of EKE naturally vanish. In the following, a more local approach is used and the eddy energy balance in Equation 3 is considered regionally, at a typical scale of $\mathcal{O}(1000)\,\mathrm{km}$.

The eddy energy balance is first validated within a global ocean model (see Text S1 of the Supporting Information for details of the numerical configuration). To summarize, the stand-alone ocean simulation includes the GEOMETRIC parameterization (Mak, Marshall, et al., 2022) which discretizes the Equation 1. Monthly means of model outputs, including each EKE trends, are stored and used to evaluate the validity of the eddy energy balance. In accordance with the climatology used in section 3, the simulation outputs are analysed over the 23-year period from 1995 to 2017. We find a slight dominance of the dissipation term over the production, leading to a modest underestimation of the eddy dissipation coefficient λ. However, the proposed diagnostic eddy energy balance is overall valid when analysing the remaining terms of Equation 1 (see Figures S1 and S2 of the Supporting Information), allowing the use of a time-averaged stratification to compute the coefficient λ. Finally, we estimate a mean relative error of 35% on the coefficient λ, a figure used to compute the uncertainty range in our results (see error and uncertainty quantification in Text S1 of the Supporting Information).

3 Eddy Dissipation from global Observations

3.1 Datasets

Retrieving the eddy dissipation rate from Equation 3 only requires an averaged large-scale density field from which the ocean stratification can be computed. For that, we use the in-situ temperature and practical salinity reconstructions from the World Ocean Atlas 2018 (WOA18) climatology (Garcia et al., 2019) to compute the conservative temperature Θ, the absolute salinity S_A and the in-situ density ρ using the TEOS-10 equation of state (IOC et al., 2010) from the GSW python toolbox (Firing et al., 2021). Then, both horizontal and vertical stratifications M^2 and N^2 are computed as:

$$M^2 = \frac{g}{\rho_0}|\nabla_h \rho| \,, \quad N^2 = \frac{g}{\rho_0}\left(\alpha_\Theta \frac{\partial \Theta}{\partial z} - \beta_S \frac{\partial S_A}{\partial z}\right), \tag{4}$$

with g the gravity acceleration, $\rho_0 = 1026$ kg/m^3 a reference density, and α_Θ and β_S the seawater thermal expansion and saline contraction coefficients respectively. A relatively large time span climatological mean is needed as the balance Equation 3 is valid typically at the large-scale and over decadal timescales. We therefore use a merge of two WOA18 datasets covering a 23-year period from 1995 to 2017, which incorporates the global Argo float measurements from 2005.

An estimation of the EKE is required to deduce the final dissipation rate defined by the second right hand side term in Equation 1. Similar to the work of Groeskamp et al. (2020), we compute the surface eddy kinetic energy from sea surface geostrophic velocity anomalies (u'_0, v'_0) with respect to the 1995-2017 period and collected at 1/4° resolution from the European Union-Copernicus Marine Service (2021). The resulting EKE map is then regridded onto the WOA18 grid while ensuring energy conservation. Since a three-dimensional energy field is needed, we apply a vertical structure function assumed to be separable so that the eddy velocity components can be formulated as $(u', v') = \phi(z)(u'_0, v'_0)$. The structure function $\phi(z)$ assumes a rough bottom topography (LaCasce & Groeskamp, 2020) and is found by solving a differential equation throughout the water column (see calculation details in Text S2 of the Supporting Information). The function $\phi(z)$ represents the variation of the eddy velocity with depth and is used to compute the depth-integrated EKE:

$$\int \mathrm{EKE}\, dz = \int \frac{\left(u_0'^2 + v_0'^2\right)}{2} \phi(z)^2 \, dz. \tag{5}$$

3.2 The Eddy Dissipation Timescale

From the WOA18 dataset, both the horizontal and vertical stratifications are computed. The integral of these metrics over the whole depth is mapped in Figure 1a,b. The horizontal stratification turns out to be a good proxy for the shear found in strong oceanic baroclinic currents, notably western boundary currents and the Antarctic Circumpolar Current (ACC). To a lesser extent, it also shows the subtropical gyre signatures and their western intensification. We also note extreme and noisy values at high latitudes, especially in the Arctic Ocean, likely due to a lack of observations during winter in the WOA18 dataset. On the other hand, the vertical stratification map shows a general equatorward increase, with regionally reduced stratification over eastern boundary upwelling systems and increased stratification in the vicinity of major river mouths. On top of that, both parameters show a strong bathymetric dependence, as they are defined as vertical integrals.

These maps help to understand the horizontal distribution of the eddy dissipation timescale λ^{-1} (units in days) obtained from Equation 3 and shown in Figure 1c. Very short eddy timescales are found near the Gulf stream, the Kuroshio and the Agulhas regions as well as along the ACC. These geographical patterns were expected since they are also regions of strong baroclinic currents. The same is also true along the north Atlantic subpolar gyre. As already pointed out in the horizontal stratification map, the short dissipation timescales found at high latitudes in the Arctic ocean and off Antarctica are doubtful. This result, although partly explained by the extremely weak vertical stratification in these regions, lacks of in-situ measurement and should be used with caution. Conversely, the dissipation timescale is large at low latitudes, in the equatorial regions and in the interior of subtropical gyres. Both the reduced horizontal shear and the high vertical stratification can explain the long eddy timescales found at those locations. To a lesser extent, a similar pattern is found in the north Pacific subpolar gyre.

This estimate can be compared to the work of Mak, Avdis, et al. (2022) who constrain the same eddy dissipation timescale using a kinematic inverse calculation inferred from an eddy permitting ocean circulation model. Similarly, short timescales are found near the western boundary currents and the ACC while subtropical gyre signatures are absent from their spatial distribution. Nevertheless, they find long dissipation timescales in eastern boundary regions, a feature less marked in our global estimation. In addition, within our eddy energy balance the eddy dissipation timescale is comparable with (although not equivalent to) the baroclinic growth rate. For instance, the eddy growth rate computed through a linear analysis by Tulloch et al. (2011) retreives similar spatial patterns, even if the present work shows higher values at mid and low latitudes.

3.3 Eddy Kinetic Energy Reconstruction

From altimetry records, the surface eddy kinetic energy is computed and averaged between 1995 and 2017. The resulting map is shown in Figure 2a. The western boundary currents, their extension, the ACC as well as the equatorial band show strong signatures with high levels of energy. The Indian Ocean also displays significant surface EKE while very weak levels are found at high latitudes, in the Arctic and next to the Antarctic, but also in the interior of subtropical gyres. The map is comparable to previous estimates of eddy kinetic energy also based on altimetry (Martinez-Moreno et al., 2020; Groeskamp et al., 2020).

Figure 2b shows the vertically-integrated EKE deduced from Equation 5. The use of the baroclinic surface mode vertical function clearly intensifies the eddy activity in the Southern Ocean while weakening the energy patterns in the tropics and subtropics. The North Atlantic Current and the Labrador Sea also display deep vertical structures which in turn reinforce the integrated EKE near the Gulf Stream extension (see Figure S4 in the Supporting Information). In addition, the bathymetry affects the final map and more particularly, almost no energy is found near the coasts nor in shallow waters.

Integrated over the whole domain, the total EKE reservoir accounts for 4.42 EJ (10^{18}J). For comparison with other studies based on high resolution models, von Storch et al. (2012) found 3.55 EJ while the work of Yu and Metzger (2019) estimated a smaller EKE reservoir of 1.76 EJ. These results therefore give credit to our method and the use of the surface mode vertical structure in the reconstruction of the geostrophic eddy field.

3.4 Global Estimate of the Eddy Kinetic Energy Dissipation

By combining the estimated eddy dissipation timescale and the vertical integral EKE, the dissipation rate of mesoscale kinetic energy is obtained and mapped in Figure 3. To some extent, the map retains the horizontal patterns of the integrated EKE (Figure 2b), although intensified. Indeed, boundary currents and the ACC are found to be highly dissipative regions of mesoscale eddies since they hold large levels of energy while also presenting short eddy dissipation timescales (Figure 1c). In the northern hemisphere, intense EKE dissipation is found in the Kuroshio as well as the Gulf Stream region and its extension. In the southern hemisphere, the Agulhas Current and its retroflection, the Zapiola gyre and the ACC signatures are striking with an eddy dissipation rate often exceeding 25 mW/m^2.

Table 1: Domain-integrated dissipation rate of the eddy kinetic energy over oceanic basins displayed in Figure 3. The longitude and latitude bounds for each box are also indicated as well as the associated ocean area. The ACC basin is defined following the mask created by Martinez-Moreno et al. (2020) but modified to include a part of the Agulhas retroflection between 52–100°E and southward to 42°S, while removing the boxes used for the southern boundary current. The surface average represents the ratio between the integrated dissipation rate and the basin area.

	Global	Gulf Stream	Kuroshio	Agulhas	Brazil-Malvinas	ACC
Longitude	-	73°-39°W	140°-175°E	14°-52°E	59.5°-32°W	-
Latitude	-	33°-44°N	30°-42°N	30°-44°S	34.5°-50.5°S	-
Surface area (10^6 km^2)	344.3	3.5	4.1	4.7	4.1	66.6
% of total	(100 %)	(1.0 %)	(1.2 %)	(1.4 %)	(1.2 %)	(19.4 %)
Dissipation rate (TW)	0.66 ± 0.19	0.05 ± 0.01	0.03 ± 0.01	0.07 ± 0.02	0.03 ± 0.01	0.25 ± 0.04
% of total	(100 %)	(7.8 ± 2.7 %)	(4.5 ± 1.8 %)	(10.6 ± 3.9 %)	(5.0 ± 2.2 %)	(37.5 ± 12.8%)
Surface average (mW/m^2)	1.93 ± 0.56	14.82 ± 2.85	7.26 ± 2.02	14.97 ± 3.42	8.06 ± 2.64	3.34 ± 0.60

The map also reveals both the East Australian Current and the West Australian Current as places of mesoscale EKE dissipation. The latter is the only ocean eastern boundary upwelling region present on this global map.

Intermediate levels of EKE dissipation are found in the equatorial and subtropical bands, mostly in the Pacific Ocean. Even if these regions are theoretically less prone to baroclinic instability (Tulloch et al., 2011), the amount of computed EKE and the simple balance of Equation 3 produce a relatively large eddy dissipation. This pattern is not often observed in previous studies (Sen et al., 2008; Xu et al., 2011) but reflects the large number of attendent eddies in these regions (Chelton et al., 2011). Finally, the dissipation rate shows strong variations zonally with very weak EKE removal in the Eastern part of ocean basins. In particular the North and South Pacific subtropical gyres have a pronounced signature with a minimum of EKE dissipation found in the vicinity of the Alaska, the California and the Humboldt Currents. Both the horizontal distribution of EKE and of the dissipation timescale explain these patterns.

Since most of the mesoscale dissipation occurs in strong and deep-reaching currents, domain-integrated EKE dissipation rates are computed over the most energetic ocean regions and summarized in Table 1. Covering only a small part of the global ocean area, the four main western boundary current systems are responsible here for more than 25% of the total EKE sinks. It is particularly true in the Agulhas and the Gulf Stream regions with an average dissipation rate of 15 mW/m^2, one order of magnitude larger than the global average. The southern hemisphere clearly dominates the EKE dissipation with numerous dissipation hotspots, notably in the ACC which cumulates more than a third of the global dissipation.

In total, we find a global EKE dissipation rate of 0.66 ± 0.19 TW. This figure represents a substantial fraction of the ∼1 TW wind power input to the geostrophic field (Wunsch, 1998) and is close to the expected eddy potential to kinetic energy conversion rate (von Storch et al., 2012), confirming the key role of mesoscale eddies in the ocean energy cycle. Our results are also in the range of previous global estimations. Sen et al. (2008) computed an observed dissipation of geostrophic motion by bottom drag between 0.2 TW and 0.8 TW while Arbic et al. (2009) obtained a reduced range of 0.14-0.65 TW from different simulations. This finding suggests the bottom drag is a leading-order mechanism of mesoscale dissipation even if regional and cross-comparison studies are needed to better quantify the EKE dissipation processes.

4 Discussion

4.1 Validition of the Eddy Energy Balance

In section 2, a diagnostic eddy energy balance is presented where the energy sources by baroclinic instability are offset by a linear EKE dissipation. In this study, we use a coarse and global low-resolution model to verify this eddy energy balance. The simulation outputs tend to validate the framework but still indicate errors evaluated at 35%. These figures should be carefully interpreted since the model and the chosen parameterized energy budget necessarily present some biases. More precisely, the barotropic instability is neglected in Equation 1 although it could be a significant mechanism for the generation of mesoscale eddies (e.g. Gula et al., 2015; Maillard et al., 2022). However, at the global scale, model-based Lorenz energy cycle estimates suggest that baroclinic production by far exceeds its barotropic counterpart (von Storch et al., 2012). In addition, satellite observations have shown that eddies could efficiently propagate westward (Chelton et al., 2007, 2011; Zhai et al., 2010), indicating that advection may play a role in the EKE budget. Finally, recent studies indicate strong observed EKE variability (Ding et al., 2017; Martinez-Moreno et al., 2020) and possible long-term trends (Beech et al., 2022). Nonetheless, on the decadal time scale relatively small trends of EKE are found, supporting the hypothesis of a steady eddy kinetic energy reservoir. In order to account for all the aforementioned processes, eddy-rich and high-resolution models could be used to validate the eddy energy balance.

4.2 Sensitivity of the Eddy Dissipation to the Eddy Efficiency α

Another assumption in our method remains in the choice of the eddy efficiency α, and to our knowledge, there is no method to get an accurate estimation of this parameter in the global ocean. Bachman et al. (2017) use a suite of idealized channel simulations to compare several parameterizations of eddy transfer coefficients. They recommend the equilibrated long-term value of 0.2, even if the eddy efficiency takes different values during the eddy lifetime. Poulsen et al. (2019) diagnose the spatial structure of the eddy efficiency in the Southern Ocean with an eddy-resolving ocean circulation model. They recommend an average value as low as 0.043, consistent with the default value of 0.04 used in the GEOMETRIC parameterization (Mak et al., 2018; Mak, Marshall, et al., 2022). More recently, Wei et al. (2022) set the eddy efficiency to 0.07 in order to optimize their diagnostics of the eddy buoyancy fluxes in shelf and open ocean regions of eddy resolving simulations.

We also note that the eddy efficiency α in Equations 2 and 3 is different from the one introduced by Marshall et al. (2012) which use the total eddy energy instead of the EKE. However, the work of Bachman et al. (2017) suggests that switching the total to eddy kinetic energy in the scaling of κ_{gm} is physically consistent even if the coefficient should be increased by a given factor. Therefore, the above-mentioned values of the eddy efficiency should be increased when considering the EKE. Therefore we chose $\alpha = 0.1$ which is around twice the mean value diagnosed by Poulsen et al. (2019) in a realistic high-resolution model. Even if this value seems reasonable, we acknowledge the large uncertainties in our results due to the linear dependences of the EKE dissipation rate to α in the Equations 1 and 3. Indeed, taking extreme values of $\alpha = 0.04$ and $\alpha = 0.4$ would lead to a central estimate of 0.27 TW and 2.66 TW respectively, for the global EKE dissipation rate.

5 Conclusion

Dominating the ocean kinetic energy reservoir, mesoscale eddies are central to the Earth energy balance and transient climate response (Greatbatch et al., 2007; Chelton, 2013). Regarding the dissipation of this eddy kinetic energy (EKE), spatial distributions are still not well quantified in the global ocean. Indeed, direct and global measurements present serious instrumental difficulties making the problem of estimating the global eddy dissipation unsolved.

This present work proposes a global reconstruction of the EKE dissipation indirectly from observations. A simplified model for the ocean mesoscale energetics is employed, where baroclinic instability sources are perfectly balanced by sinks of EKE. In this model, the dissipative mechanisms are interpreted by means of eddy dissipation timescales and are directly related to the ocean stratification. The model and the energy balance were tested with an oceanic global circulation simulation using a parameterized eddy energy prognostic equation. In the whole ocean domain, the dissipation of EKE tends to approach its production by baroclinic instability, thereby confirming the adopted eddy energy balance. However, the dissipation also dominates some part of the ocean where other processes impact the EKE budget, illustrating the need for more realistic diagnostics of this eddy energy balance.

The framework is applied to available observations of temperature and salinity to compute a global map of the eddy dissipation timescale. The shortest timescales (higher dissipation) are found in the Southern Ocean and near strong western boundary currents coinciding with the regions prone to high baroclinic instability and large eddy growth rates (Tulloch et al., 2011). By projecting the eddy energy into depth using baroclinic surface modes (LaCasce & Groeskamp, 2020), a three-dimensional EKE field is also computed where the mean EKE reservoir is estimated to 4.42 EJ. Our work finally combines the two previous ingredients and provides a new global map for the EKE dissipation rate. Integrated over the whole ocean, the energy flux going out of the mesoscale reaches 0.66 ± 0.19 TW. Our study also confirms that most of the energy dissipation takes place in the southern hemisphere and more particularly in the Antarctic Circumpolar Current which accounts for 38% of the total dissipation. In addition, the main western boundary currents are found to be dissipation hotspots of EKE, accounting for more than 25% of the global dissipation.

Given the simplicity of the relation in Equation 3, the adopted framework allows an easy computation of the global EKE dissipation rate from indirect observations. Indeed, the method only requires a climatological mean field of density and surface geostrophic velocity anomalies, both of these being widely available observational data. Our results show important spatial patterns which if combined with other independent estimates, can help to understand the dissipation mechanisms. Since the dissipation of geostrophic kinetic energy remains one of the largest uncertainties in the ocean energy budget (Wunsch, 2004), it is thus crucial to quantify how and where the energy is removed from the EKE reservoir. Our results contribute to this goal and provide a new spatial distribution of the EKE dissipation rate in the world ocean.

Another important finding of this work is the estimation of the linear eddy dissipation coefficient λ employed in several ocean models (Cessi, 2008; Marshall & Adcroft, 2010; Mak et al., 2017, 2018). Recently, Mak, Marshall, et al. (2022) have demonstrated the sensitivity of global ocean circulation models using energy constrained mesoscale eddy parameterization to the eddy dissipation timescale λ^{-1}. In this study, we present the first estimate of the eddy timescale from global observation-based datasets. The resulting map can thus be used in eddy-parameterized ocean models to constrain the eddy energy dissipation and modulate the ocean stratification.

Open Research

This study has been conducted using E.U. Copernicus Marine Service Information: `https://doi.org/10.48670/moi-00148` for the altimetry dataset. Both climatology of temperature (Locarnini et al., 2018) and salinity (Zweng et al., 2018) from the World Ocean Atlas 2018 were downloaded through the National Oceanic and Atmospheric Administration website: `https://www.ncei.noaa.gov/archive/accession/NCEI-WOA18`, on 9 September

2022. Datas and Python scripts used to generate the results presented in this work are available on Zenodo : `https://sandbox.zenodo.org/record/1206326`.

Acknowledgments

This project has received support from the European Union's Horizon 2020 research and innovation programme under Grant Agreement N° 101003536 (ESM2025 – Earth System Models for the Future). JM also acknowledges support from both the RGC Early Career Scheme 2630020 and the Center for Ocean Research in Hong Kong and Macau, a joint research center between the Qingdao National Laboratory for Marine Science and Technology and Hong Kong University of Science and Technology. The authors would like to thank Sjoerd Groeskamp for his review and useful comments, and Jean-Baptiste Sallée for the discussions about observational measurements that make improvements in this final version of the article.

References

Arbic, B. K., Shriver, J. F., Hogan, P. J., Hurlburt, H. E., McClean, J. L., Metzger, E. J., . . . Wallcraft, A. J. (2009, feb). Estimates of bottom flows and bottom boundary layer dissipation of the oceanic general circulation from global high-resolution models. *Journal of Geophysical Research*, *114*(C2). doi: 10.1029/2008jc005072

Bachman, S., Marshall, D., Maddison, J., & Mak, J. (2017). Evaluation of a scalar eddy transport coefficient based on geometric constraints. *Ocean Modelling*, *109*, 44–54. doi: 10.1016/j.ocemod.2016.12.004

Barkan, R., Winters, K. B., & Smith, S. G. L. (2015, jan). Energy cascades and loss of balance in a reentrant channel forced by wind stress and buoyancy fluxes. *Journal of Physical Oceanography*, *45*(1), 272–293. doi: 10.1175/JPO-D-14-0068.1

Beech, N., Rackow, T., Semmler, T., Danilov, S., Wang, Q., & Jung, T. (2022, sep). Long-term evolution of ocean eddy activity in a warming world. *Nature Climate Change*, *12*(10), 910–917. doi: 10.1038/s41558-022-01478-3

Braby, L., Backeberg, B. C., Ansorge, I., Roberts, M. J., Krug, M., & Reason, C. J. C. (2016, aug). Observed eddy dissipation in the Agulhas Current. *Geophysical Research Letters*, *43*(15), 8143–8150. doi: 10.1002/2016gl069480

Cessi, P. (2008, aug). An energy-constrained parameterization of eddy buoyancy flux. *Journal of Physical Oceanography*, *38*(8), 1807–1819. doi: 10.1175/2007JPO3812.1

Chelton, D. B. (2013, jul). Mesoscale eddy effects. *Nature Geoscience*, *6*(8), 594–595. doi: 10.1038/ngeo1906

Chelton, D. B., Schlax, M. G., & Samelson, R. M. (2011, oct). Global observations of nonlinear mesoscale eddies. *Progress in Oceanography*, *91*(2), 167–216. doi: 10.1016/j.pocean.2011.01.002

Chelton, D. B., Schlax, M. G., Samelson, R. M., & de Szoeke, R. A. (2007, aug). Global observations of large oceanic eddies. *Geophysical Research Letters*, *34*(15). doi: 10.1029/2007gl030812

Cooley, S., Schoeman, D., Bopp, L., Boyd, P., Donner, S., Ghebrehiwet, D., . . . Skern-Mauritzen, M. (2022). Oceans and coastal ecosystems and their services. in: Climatechange 2022: Impacts, adaptation and vulnerability. contribution of working group ii to the sixth assessment report ofthe intergovernmental panel on climate change. In H.-O. Pörtner et al. (Eds.), (p. 379–550). Cambridge University Press, Cambridge,UK and New York, NY, USA. Retrieved from `https://www.ipcc.ch/report/ar6/wg2/downloads/report`

Couldrey, M. P., Gregory, J. M., Dias, F. B., Dobrohotoff, P., Domingues, C. M., Garuba, O., . . . Zanna, L. (2020, oct). What causes the spread of model projections of ocean dynamic sea-level change in response to greenhouse gas forcing? *Climate Dynamics*, *56*(1-2), 155–187. doi: 10.1007/s00382-020-05471-4

Ding, M., Lin, P., Liu, H., & Chai, F. (2017, dec). Increased eddy activity in the northeastern Pacific during 1993–2011. *Journal of Climate*, *31*(1), 387–399. doi: 10.1175/jcli-d-17-0309.1

European Union-Copernicus Marine Service. (2021). *Global ocean gridded l4 sea surface heights and derived variables reprocessed (1993-ongoing).* Mercator Ocean International. doi: 10.48670/MOI-00148

Ferrari, R., & Wunsch, C. (2009, jan). Ocean circulation kinetic energy: Reservoirs, sources, and sinks. *Annual Review of Fluid Mechanics*, *41*(1), 253–282. doi: http://dx.doi.org/10.1146/annurev.fluid.40.111406.102139

Firing, E., , Filipe, Barna, A., & Abernathey, R. (2021). *Teos-10/gsw-python: v3.4.1.* Zenodo. Retrieved from `https://teos-10.github.io/GSW-Python/` doi: 10.5281/ZENODO.4631364

Fox-Kemper, B., Adcroft, A., Böning, C. W., Chassignet, E. P., Curchitser, E., Danabasoglu, G., . . . Yeager, S. G. (2019, feb). Challenges and prospects in ocean circulation models. *Frontiers in Marine Science*, *6*. doi: 10.3389/fmars.2019.00065

Fox-Kemper, B., Hewitt, H., Xiao, C., Adalgeirsdóttir, G., Drijfhout, S., Edwards, T., . . . Yu, Y. (2021). Ocean, cryosphere and sea level change. in climate change 2021: The physical science basis. contribution of working group i to the sixth assessment report of the intergovernmental panel on climate change. In M.-D. V. et al. (Eds.), (p. 1211–1362). Cambridge University Press,Cambridge, United Kingdom and New York, NY, USA. Retrieved from `https://www.ipcc.ch/report/ar6/wg1/chapter/chapter-9/`

Friedlingstein, P., Jones, M. W., O'Sullivan, M., Andrew, R. M., Bakker, D. C. E., Hauck, J., . . . Zeng, J. (2022, apr). Global carbon budget 2021. *Earth System Science Data*, *14*(4), 1917–2005. doi: 10.5194/essd-14-1917-2022

Garcia, H. E., Boyer, T. P., Baranova, O. K., Locarnini, R. A., Mishonov, A. V., Grodsky, A., . . . Zweng, M. M. (2019). World Ocean Atlas 2018: Product documentation. *NOAA National Centers for Environmental Information*. Retrieved from `https://www.ncei.noaa.gov/archive/accession/NCEI-WOA18`

Gent, P. R., & McWilliams, J. C. (1990, jan). Isopycnal mixing in ocean circulation models. *Journal of Physical Oceanography*, *20*(1), 150-155. doi: 10.1175/1520-0485(1990)020⟨0150:imiocm⟩2.0.co;2

Gent, P. R., Willebrand, J., McDougall, T. J., & McWilliams, J. C. (1995, apr). Parameterizing eddy-induced tracer transports in ocean circulation models. *Journal of Physical Oceanography*, *25*(4), 463–474. doi: 10.1175/1520-0485(1995)025⟨0463:peitti⟩2.0.co;2

Greatbatch, R. J., Zhai, X., Eden, C., & Olbers, D. (2007, apr). The possible role in the ocean heat budget of eddy-induced mixing due to air-sea interaction. *Geophysical Research Letters*, *34*(7). doi: 10.1029/2007gl029533

Groeskamp, S., LaCasce, J. H., McDougall, T. J., & Rogé, M. (2020, sep). Full-depth global estimates of ocean mesoscale eddy mixing from observations and theory. *Geophysical Research Letters*, *47*(18). Retrieved from `https://doi.org/10.1029/2020GL089425` doi: 10.1029/2020gl089425

Gula, J., Molemaker, M. J., & McWilliams, J. C. (2015, mar). Gulf Stream dynamics along the southeastern U.S. seaboard. *Journal of Physical Oceanography*, *45*(3), 690–715. doi: 10.1175/jpo-d-14-0154.1

IOC, SCOR, & IAPSO. (2010). The international thermodynamic equation of seawater – 2010: Calculation and use of thermodynamic properties. In (p. 196). UNESCO (English).

Ji, J., Dong, C., Zhang, B., Liu, Y., Zou, B., King, G. P., . . . Chen, D. (2018, nov). Oceanic eddy characteristics and generation mechanisms in the Kuroshio extension region. *Journal of Geophysical Research: Oceans*, *123*(11), 8548–8567. doi: 10.1029/2018jc014196

Klymak, J. M. (2018, oct). Nonpropagating form drag and turbulence due to stratified flow over large-scale abyssal hill topography. *Journal of Physical Oceanography*, *48*(10), 2383–2395. doi: 10.1175/jpo-d-17-0225.1

Klymak, J. M., Balwada, D., Garabato, A. N., & Abernathey, R. (2021, may). Parameterizing nonpropagating form drag over rough bathymetry. *Journal of Physical Oceanography*, *51*(5), 1489–1501. doi: 10.1175/jpo-d-20-0112.1

LaCasce, J. H., & Groeskamp, S. (2020, oct). Baroclinic modes over rough bathymetry and the surface deformation radius. *Journal of Physical Oceanography*, *50*(10), 2835–2847. doi: 10.1175/jpo-d-20-0055.1

Locarnini, R. A., Mishonov, A. V., Baranova, O. K., Boyer, T. P., Zweng, M. M., García, H. E., ... Smolyar, I. (2018). World Ocean Atlas 2018, Volume 1: Temperature. *NOAA Atlas NESDIS*(81), 52.

Maillard, L., Boucharel, J., & Renault, L. (2022, aug). Direct and rectified effects of tropical instability waves on the eastern tropical Pacific mean state in a regional ocean model. *Journal of Physical Oceanography*, *52*(8), 1817–1834. doi: 10.1175/jpo-d-21-0300.1

Mak, J., Avdis, A., David, T., Lee, H. S., Na, Y., Wang, Y., & Yan, F. E. (2022). On constraining the mesoscale eddy energy dissipation time-scale. *Journal of Advances in Modeling Earth Systems*. doi: https://doi.org/10.1029/2022MS003223

Mak, J., Maddison, J. R., Marshall, D. P., & Munday, D. R. (2018, oct). Implementation of a geometrically informed and energetically constrained mesoscale eddy parameterization in an ocean circulation model. *Journal of Physical Oceanography*, *48*(10), 2363–2382. doi: 10.1175/jpo-d-18-0017.1

Mak, J., Marshall, D., Maddison, J., & Bachman, S. (2017, apr). Emergent eddy saturation from an energy constrained eddy parameterisation. *Ocean Modelling*, *112*, 125–138. doi: http://dx.doi.org/10.1016/j.ocemod.2017.02.007

Mak, J., Marshall, D. P., Madec, G., & Maddison, J. R. (2022, apr). Acute sensitivity of global ocean circulation and heat content to eddy energy dissipation timescale. *Geophysical Research Letters*, *49*(8). doi: 10.1029/2021GL097259

Marshall, D. P., & Adcroft, A. J. (2010, jan). Parameterization of ocean eddies: Potential vorticity mixing, energetics and Arnold's first stability theorem. *Ocean Modelling*, *32*(3-4), 188–204. doi: 10.1016/j.ocemod.2010.02.001

Marshall, D. P., Ambaum, M. H. P., Maddison, J. R., Munday, D. R., & Novak, L. (2017, jan). Eddy saturation and frictional control of the Antarctic Circumpolar Current. *Geophysical Research Letters*, *44*(1), 286–292. doi: 10.1002/2016gl071702

Marshall, D. P., Maddison, J. R., & Berloff, P. S. (2012, apr). A framework for parameterizing eddy potential vorticity fluxes. *Journal of Physical Oceanography*, *42*(4), 539–557. doi: 10.1175/jpo-d-11-048.1

Martinez-Moreno, J., Hogg, A., England, M., Constantinou, N. C., Kiss, A. E., & Morrison, A. (2020, oct). Global changes in oceanic mesoscale currents over the satellite altimetry record.
doi: 10.21203/rs.3.rs-88932/v1

McWilliams, J. C. (2016, may). Submesoscale currents in the ocean. *Proceedings of the Royal Society A: Mathematical, Physical and Engineering Sciences*, *472*(2189), 20160117. doi: 10.1098/rspa.2016.0117

Melet, A., Hallberg, R., Adcroft, A., Nikurashin, M., & Legg, S. (2015, mar). Energy flux into internal lee waves: Sensitivity to future climate changes using linear theory and a climate model. *Journal of Climate*, *28*(6), 2365–2384. doi: 10.1175/jcli-d-14-00432.1

Molemaker, M. J., McWilliams, J. C., & Capet, X. (2010, jun). Balanced and unbalanced routes to dissipation in an equilibrated Eady flow. *Journal of Fluid Mechanics*, *654*, 35–63. doi: 10.1017/S0022112009993272

Naveira Garabato, A. C., Polzin, K. L., King, B. A., Heywood, K. J., & Visbeck, M. (2004, jan). Widespread intense turbulent mixing in the southern ocean. *Science*, *303*(5655), 210–213. doi: 10.1126/science.1090929

Nikurashin, M., & Ferrari, R. (2011, apr). Global energy conversion rate from geostrophic flows into internal lee waves in the deep ocean. *Geophysical Research Letters*, *38*(8). doi: 10.1029/2011GL046576

Polzin, K. L. (2010, apr). Mesoscale eddy–internal wave coupling. part II: Energetics and results from PolyMode. *Journal of Physical Oceanography*, *40*(4), 789–801. doi:

10.1175/2009jpo4039.1

Poulsen, M. B., Jochum, M., Maddison, J. R., Marshall, D. P., & Nuterman, R. (2019). A geometric interpretation of southern ocean eddy form stress. *Journal of Physical Oceanography*, *49*(10), 2553–2570. doi: 10.1175/JPO-D-18-0220.1

Rai, S., Hecht, M., Maltrud, M., & Aluie, H. (2021, jul). Scale of oceanic eddy killing by wind from global satellite observations. *Science Advances*, *7*(28). doi: 10.1126/sciadv.abf4920

Renault, L., Marchesiello, P., Masson, S., & McWilliams, J. C. (2019, mar). Remarkable control of western boundary currents by *eddy killing*, a mechanical air-sea coupling process. *Geophysical Research Letters*, *46*(5), 2743–2751. doi: 10.1029/2018gl081211

Robinson, A. R., & McWilliams, J. C. (1974, jul). The baroclinic instability of the open ocean. *Journal of Physical Oceanography*, *4*(3), 281–294. doi: 10.1175/1520-0485(1974)004⟨0281:TBIOTO⟩2.0.CO;2

Saenko, O. A., Yang, D., & Gregory, J. M. (2018, oct). Impact of mesoscale eddy transfer on heat uptake in an eddy-parameterizing ocean model. *Journal of Climate*, *31*(20), 8589–8606. doi: 10.1175/jcli-d-18-0186.1

Saenko, O. A., Zhai, X., Merryfield, W. J., & Lee, W. G. (2012, apr). The combined effect of tidally and eddy-driven diapycnal mixing on the large-scale ocean circulation. *Journal of Physical Oceanography*, *42*(4), 526–538. doi: 10.1175/jpo-d-11-0122.1

Scott, R. B., Goff, J. A., Garabato, A. C. N., & Nurser, A. J. G. (2011, sep). Global rate and spectral characteristics of internal gravity wave generation by geostrophic flow over topography. *Journal of Geophysical Research*, *116*(C9). doi: 10.1029/2011jc007005

Sen, A., Scott, R. B., & Arbic, B. K. (2008, may). Global energy dissipation rate of deep-ocean low-frequency flows by quadratic bottom boundary layer drag: Computations from current-meter data. *Geophysical Research Letters*, *35*(9). doi: 10.1029/2008GL033407

Sun, M., Tian, F., Liu, Y., & Chen, G. (2017, feb). An improved automatic algorithm for global eddy tracking using satellite altimeter data. *Remote Sensing*, *9*(3), 206. doi: 10.3390/rs9030206

Tulloch, R., Marshall, J., Hill, C., & Smith, K. S. (2011, jun). Scales, growth rates, and spectral fluxes of baroclinic instability in the ocean. *Journal of Physical Oceanography*, *41*(6), 1057–1076. doi: 10.1175/2011jpo4404.1

von Schuckmann, K., Cheng, L., Palmer, M. D., Hansen, J., Tassone, C., Aich, V., ... Wijffels, S. E. (2020, sep). Heat stored in the earth system: where does the energy go? *Earth System Science Data*, *12*(3), 2013–2041. doi: 10.5194/essd-12-2013-2020

von Storch, J.-S., Eden, C., Fast, I., Haak, H., Hernández-Deckers, D., Maier-Reimer, E., ... Stammer, D. (2012, dec). An estimate of the Lorenz energy cycle for the world ocean based on the STORM/NCEP simulation. *Journal of Physical Oceanography*, *42*(12), 2185–2205. doi: https://doi.org/10.1175/JPO-D-12-079.1

Wei, H., Wang, Y., Stewart, A. L., & Mak, J. (2022, dec). Scalings for eddy buoyancy fluxes across prograde shelf/slope fronts. *Journal of Advances in Modeling Earth Systems*, *14*(12). doi: 10.1029/2022ms003229

Wunsch, C. (1998, nov). The work done by the wind on the oceanic general circulation. *Journal of Physical Oceanography*, *28*(11), 2332–2340. doi: 10.1175/1520-0485(1998)028⟨2332:twdbtw⟩2.0.co;2

Wunsch, C. (2004, jan). Vertical mixing, energy, and the general circulation of the oceans. *Annual Review of Fluid Mechanics*, *36*(1), 281–314. doi: 10.1146/annurev.fluid.36.050802.122121

Xu, C., Shang, X.-D., & Huang, R. X. (2011, feb). Estimate of eddy energy generation/dissipation rate in the world ocean from altimetry data. *Ocean Dynamics*, *61*(4), 525–541. doi: 10.1007/s10236-011-0377-8

Yang, Q., Nikurashin, M., Sasaki, H., Sun, H., & Tian, J. (2019, jan). Dissipation of mesoscale eddies and its contribution to mixing in the northern South China Sea. *Scientific Reports*, *9*(1). doi: 10.1038/s41598-018-36610-x

Yu, Z., & Metzger, E. J. (2019, jul). The impact of ocean surface currents on global eddy kinetic energy via the wind stress formulation. *Ocean Modelling*, *139*, 101399. doi: 10.1016/j.ocemod.2019.05.003

Zanna, L., Khatiwala, S., Gregory, J. M., Ison, J., & Heimbach, P. (2019, jan). Global reconstruction of historical ocean heat storage and transport. *Proceedings of the National Academy of Sciences*, *116*(4), 1126–1131. doi: 10.1073/pnas.1808838115

Zhai, X., Johnson, H. L., & Marshall, D. P. (2010, aug). Significant sink of ocean-eddy energy near western boundaries. *Nature Geoscience*, *3*(9), 608–612. doi: https://doi.org/10.1038/ngeo943

Zweng, M. M., Reagan, J. R., Seidov, D., Boyer, T. P., Locarnini, R. A., García, H. E., … Smolyar, I. (2018). World Ocean Atlas 2018, Volume 2: Salinity. *NOAA Atlas NESDIS*(82), 50.

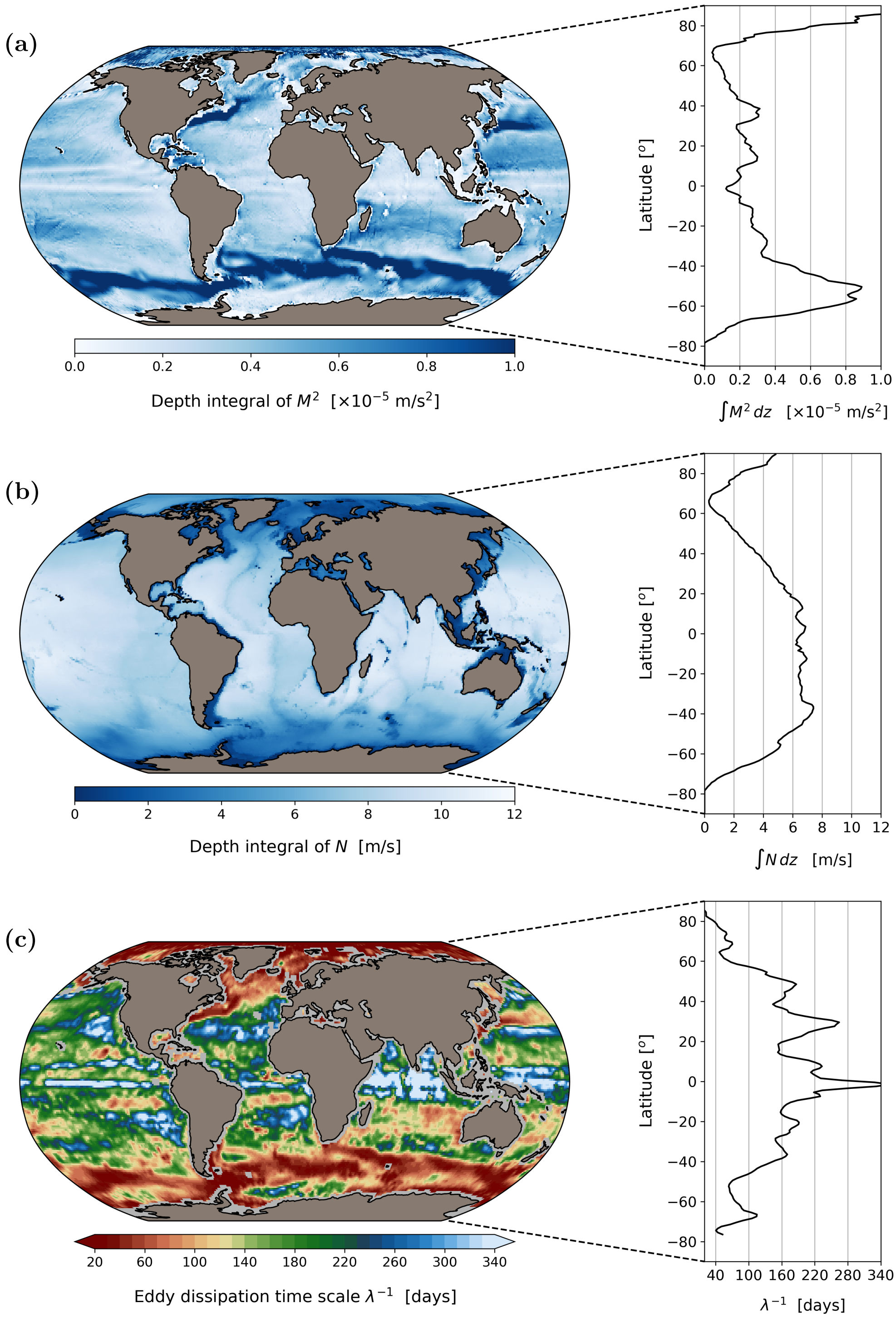

Figure 1: Depth integrals of (a) the horizontal buoyancy stratification M^2 (m/s^2) and (b) the Brunt-Väisälä frequency N (m/s) from the WOA18 climatology (Garcia et al., 2019). Equation 3 is used to compute (c) the global map of the eddy dissipation timescale λ^{-1} involving the ratio M^2/N while zonal averages are plotted on the right. In (a, b), the colormap is chosen so that dark blue leads to an increase of the eddy dissipation coefficient λ and conversely for light blue. In (c), we use a two-dimensional shapiro filter to reduce spatial noise.

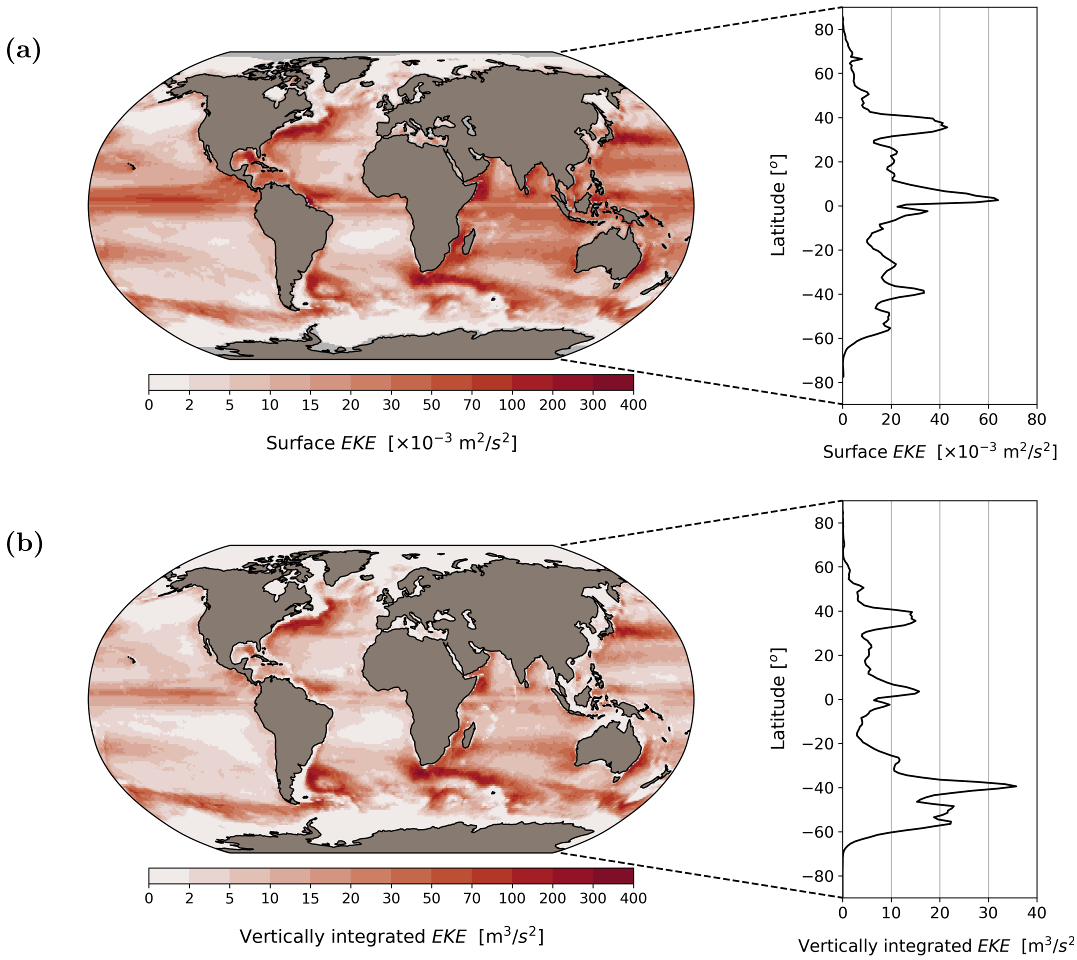

Figure 2: (a) Surface eddy kinetic energy (EKE) in $\mathrm{m}^2/\mathrm{s}^2$ deduced from the gridded altimetry (European Union-Copernicus Marine Service, 2021) and averaged over the period 1995–2017. (b) Vertically integrated EKE in $\mathrm{m}^3/\mathrm{s}^2$ deduced from the vertical structure function $\phi(z)$ in Equation 5. Both colorbars are chosen to illustrate the impact of $\phi(z)$ when computing the depth integral of EKE.

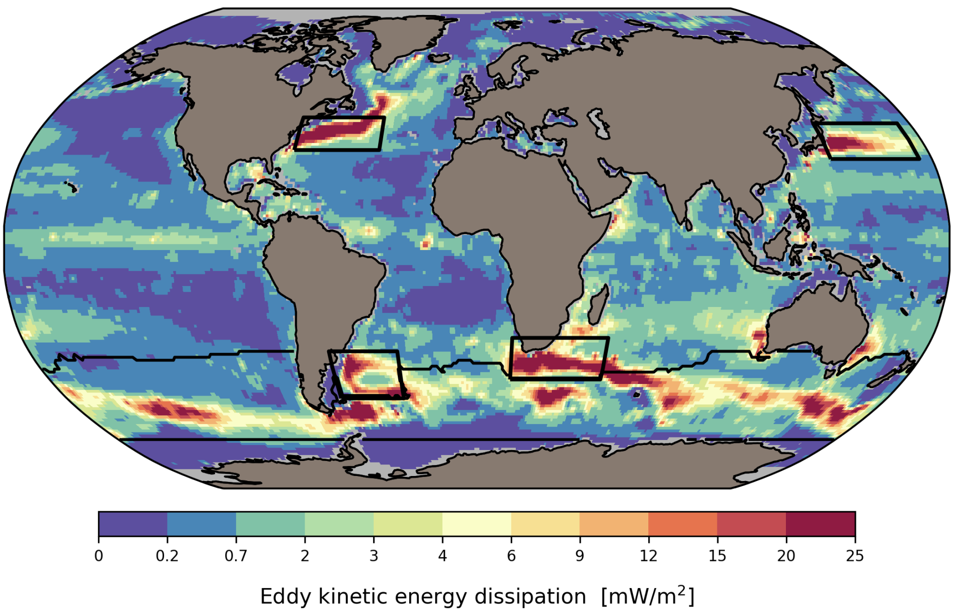

Figure 3: Vertically-integrated eddy dissipation rate in $\mathrm{mW/m^2}$ estimated from the WOA18 climatology (Garcia et al., 2019) and the gridded altimetry (European Union-Copernicus Marine Service, 2021) over the period 1995–2017, with the use of the diagnostic relation in Equation 3. A reference density $\rho_0 = 1026$ $\mathrm{kg/m^3}$ is used and the black boxes refer to the ocean basins defined in Table 1.

Supporting Information for "Global estimate of the eddy kinetic energy dissipation from a diagnostic energy balance"

Romain Torres[1], Robin Waldman[1], Julian Mak[2,3], Roland Séférian[1]

[1]CNRM, Université de Toulouse, Météo-France, CNRS, Toulouse, France

[2]Department of Ocean Science, Hong Kong University of Science and Technology, Hong Kong

[3]Center for Ocean Research in Hong Kong and Macau, Hong Kong University of Science and Technology, Hong Kong

Contents of this file

Text S1: Parameterized eddy energy budget in a global ocean model

The NEMO-OMIP2 simulation

The simple eddy energy balance of Equation 3 presented in the main document is first validated within a global ocean model. For this purpose, we use a global OMIP2 hindcast simulation over the period 1958–2018 (Voldoire, 2020). The ocean circulation is solved by NEMO (Nucleus for European Models of the Oceans) version 3.6 (Madec et al., 2017), with the embedded sea ice module GELATO version 6 (Mélia, 2002). An eORCA1 grid is used with a nominal resolution of 1° within the tripolar curvilinear ORCA grid. The model employs 75 vertical levels in z-coordinate and uses the Roquet, Madec, McDougall, and Barker (2015) TEOS-10 approximation for the seawater thermodynamics.

At the air-sea interface, the model is forced at hourly frequency by the Japanese 55-year atmospheric reanalysis for driving ocean models (JRA55-do v1.5.0; Tsujino et al., 2018), using bulk forcing. The experiment is configured in accordance with the 61-year (1958-2018) cycle defined by the OMIP-2 protocol (Tsujino et al., 2020). The simulation was first spun up for three cycles without solving any eddy kinetic energy budget before using the GEOMETRIC parameterization (Mak et al., 2022) for three more cycles. The latter discretizes the EKE budget in Equation 1 and redefines the eddy transport coefficient κ_{gm} accordingly (see the implementation details in the Supporting Information of Mak et al., 2022).

The NEMO-OMIP2 outputs are time-averaged from 1993 to 2017 and then used to analyse the EKE budget. Figure S1 shows the maps for the depth integrated EKE and the associated trends. The dissipation and production terms display similar but opposite patterns confirming the eddy energy balance. In the regions of high EKE horizontal gradients such as the western boundary currents and some spots along the Antarctic Circumpolar Current (ACC), the diffusion term reaches relatively large values even if it is not necessarily the most prominent term. The effect of the advection trend is here particularly minor while the total temporal derivative of EKE is low and contained in highly energetic currents.

Evidence of the eddy energy balance

Using the time-averaged outputs from the NEMO-OMIP2 simulation, the ratio between the baroclinic production and linear dissipation is shown in Figure S2. The energy balance is valid in most part of the ocean area where the ratio "production / dissipation" tend to be close to unity. The diagnostic balance breaks down along the equator, near continental boundaries and locally at mid to high latitudes. These features are mainly explained when analysing the remaining terms of Equation 1 (Figure S1). Along boundaries and at mid to high latitudes, the large levels of energy drive a significant horizontal EKE diffusion which locally breaks the balance. Along the equator, the eddy energy reaches its minimum value leading to a meridional gradient of EKE and thus the diffusion is again non-negligible. However, the largest errors ($> 35\%$) on the eddy energy balance are contained near the coast or at high latitudes, where the EKE is extremely weak.

Method uncertainty quantifications

The computation of the linear eddy kinetic energy dissipation rate λ is based on two main assumptions: 1) the baroclinic production is fully balanced by the linear dissipation and 2) the eddy energy balance can be retrieved from the time averaged ocean stratification. In this section, we detail the method to obtain the uncertainties from these two hypothesis using the NEMO-OMIP2 simulation outputs. However, the modelling choices already described in the main document which result in the formulation of the baroclinic production and the linear dissipation are not discussed.

1. Assuming the eddy energy balance is exact over a given time period leads to the following equality:

$$\overline{P_e} = \lambda \overline{\int \mathrm{EKE}\, dz}, \tag{SI-1}$$

where P_e is the baroclinic production saved online by the model and $\overline{}$ denotes for a time averaging operator during the given time period. From this equation, one can compute the dissipation coefficient:

$$\lambda_{\mathrm{bal}} = \frac{\overline{P_e}}{\overline{\int \mathrm{EKE}\, dz}}, \tag{SI-2}$$

Thus, λ_{bal} represents the eddy dissipation rate computed directly from the assumed eddy energy balance and gives the first source of errors when compared to the prescribed *true* λ.

2. The true time averaged production term computed by the model is given by :

$$\overline{P_e} = \alpha \overline{\left(\frac{\int (M^4/N^2)\, dz}{\int (M^2/N)\ dz} \cdot \int \mathrm{EKE}\, dz \right)}, \tag{SI-3}$$

However, from an observation-based climatology of ocean temperature and salinity, only the averaged squared horizontal and vertical buoyancy frequencies $\overline{M^2}$ and $\overline{N^2}$ can be computed. We then use the following formulation to estimate errors arising from the time average approximation :

$$\lambda_{\mathrm{av}} = \alpha \frac{\int \left(\overline{M^2}^2 / \overline{N^2} \right) dz}{\int \left(\overline{M^2} / \sqrt{\overline{N^2}} \right) dz}, \tag{SI-4}$$

where $\overline{M^2}$ and $\overline{N^2}$ are also diagnosed online. λ_{av} can then be compared to both λ_{bal} and the prescribed λ to give errors from the time average approximation only and the total (time average + energy balance hypothesis) respectively.

Both errors are mapped in Figure S3. As expected, the eddy energy balance error map is similar in patterns and amplitudes to the ratio between the averaged production and linear dissipation displayed in Figure S2. In contrast, errors from the time averaging operation show high horizontal dependence with an underestimated λ (negative errors) at lower latitudes and a large overestimation (positive errors) near coastal boundaries. Moreover, errors from the time averaging are low in the Southern Ocean.

The mean relative errors are estimated to 18% for the eddy energy balance and 17% for the time-averaging processing. Combined, a total of 35% error on the eddy dissipation coefficient λ is found, leading to the uncertainty range in our final global EKE dissipation estimate.

As discussed in the main document, this error calculation is based on the model outputs and therefore already includes some biases due to numerical choices in the GEOMETRIC parameterization. Nevertheless, assuming the eddy energy budget and the ocean stratification evolution are to a first order well approximated by the NEMO-OMIP2 simulation, the errors presented here can give an overall idea of the uncertainties for the resulting eddy dissipation rate λ. Since the spatial distribution is model-dependent, an overall metric is needed to be applied in other climatologies and datasets. Thus we computed, two uncertainties for the eddy dissipation rate λ, noted δ_{av} and δ_{bal} using a 68.3% confidence interval (or one standard deviation from the mean):

$$p\left(|\lambda_{\mathrm{av}} - \lambda_{\mathrm{bal}}| < \delta_{\mathrm{av}}\right) = 0.683 \quad \& \quad p\left(|\lambda_{\mathrm{bal}} - \lambda| < \delta_{\mathrm{bal}}\right) = 0.683. \tag{SI-5}$$

where p represents the probability or the percentage of ocean cells where the absolute error is bellow a given level. The Table S1 summarizes the resulting errors and uncertainties from the two identified sources.

Text S2: Computing the vertical structure function $\phi(z)$

The vertical structure fonction is obtained from the World Ocean Atlas 2018 (WOA18) climatology (Garcia et al., 2019) following the method described in LaCasce and Groeskamp (2020); Groeskamp, LaCasce, McDougall, and Rogé (2020). Assuming the mesoscale velocity field is well represented by the linear Quasi-Geostrophic potential vorticity equation and the Brunt-Väisälä frequency N is a function of depth only yields an equation for the vertical structure $\phi(z)$:

$$\frac{d}{dz}\left(\frac{1}{N^2}\frac{d\phi}{dz}\right)+\frac{1}{c}\,\phi=0, \tag{SI-6}$$

where c is a surface mode gravity wave phase speed and is initially not known. For the surface boundary condition, a rigid surface is set where the vertical velocity and so $d\phi/dz$ vanishes. By convention, we also fix the condition $\phi(z=0)=1$ at the surface. Then a rough bottom boundary condition is considered with zero velocity so that $\phi(z=-H)=0$. The Equation SI-6 is then solved iteratively from the surface to the bottom using a Runge-Kutta-4 integration method. An initial guess is needed for the gravity wave phase speeds and for that we use:

$$c_{\text{guess}}=\frac{1.5}{\pi}\int_{-H}^{0}N(z)\,dz. \tag{SI-7}$$

Then, a Newton method iterative algorithm is used to adjust the phase speed until the bottom condition with zero velocity is statisfied. The coefficient 1.5 in Equation SI-7 is chosen to improve the convergence. In total, 99.01 % of the profiles converged quickly after 10 iterations. The remaining unconverged profiles are mostly localised at very high latitudes or close to the coast, and are thus removed when computing the EKE dissipation rate without impacting the results.

Figure S4 shows the e-folding decreasing EKE depth represented by the depth where the squared vertical structure function ϕ^2 equals 0.37. Consistent with Groeskamp et al. (2020), the main patterns are retreived. Notably, low latitudes and shallow waters are home to surface-intensified currents while the Southern Ocean and the Gulf Stream extension area have deeper signatures. However by focusing on the squared vertical function ϕ^2 and the EKE instead of the eddy velocities, our map shows stronger latitude dependance.

References

Garcia, H. E., Boyer, T. P., Baranova, O. K., Locarnini, R. A., Mishonov, A. V., Grodsky, A., ... Zweng, M. M. (2019). World Ocean Atlas 2018: Product documentation. *NOAA National Centers for Environmental Information*. Retrieved from `https://www.ncei.noaa.gov/archive/accession/NCEI-WOA18`

Groeskamp, S., LaCasce, J. H., McDougall, T. J., & Rogé, M. (2020, sep). Full-depth global estimates of ocean mesoscale eddy mixing from observations and theory. *Geophysical Research Letters*, *47*(18). Retrieved from `https://doi.org/10.1029/2020GL089425` doi: 10.1029/2020gl089425

LaCasce, J. H., & Groeskamp, S. (2020, oct). Baroclinic modes over rough bathymetry and the surface deformation radius. *Journal of Physical Oceanography*, *50*(10), 2835–2847. doi: 10.1175/jpo-d-20-0055.1

Madec, G., Bourdallé-Badie, R., Pierre-Antoine Bouttier, Bricaud, C., Bruciaferri, D., Calvert, D., ... Vancoppenolle, M. (2017). NEMO ocean engine. Retrieved from https://doi.org/10.5281/zenodo.1472492 doi: 10.5281/ZENODO.1472492

Mak, J., Marshall, D. P., Madec, G., & Maddison, J. R. (2022, apr). Acute sensitivity of global ocean circulation and heat content to eddy energy dissipation timescale. *Geophysical Research Letters*, *49*(8). doi: 10.1029/2021GL097259

Mélia, D. S. (2002, jan). A global coupled sea ice–ocean model. *Ocean Modelling*, *4*(2), 137–172. doi: 10.1016/s1463-5003(01)00015-4

Roquet, F., Madec, G., McDougall, T. J., & Barker, P. M. (2015, jun). Accurate polynomial expressions for the density and specific volume of seawater using the TEOS-10 standard. *Ocean Modelling*, *90*, 29–43. doi: http://dx.doi.org/10.1016/j.ocemod.2015.04.002

Tsujino, H., Urakawa, L. S., Griffies, S. M., Danabasoglu, G., Adcroft, A. J., Amaral, A. E., ... Yu, Z. (2020, aug). Evaluation of global ocean–sea-ice model simulations based on the experimental protocols of the ocean model intercomparison project phase 2 (OMIP-2). *Geoscientific Model Development*, *13*(8), 3643–3708. doi: 10.5194/gmd-13-3643-2020

Tsujino, H., Urakawa, S., Nakano, H., Small, R. J., Kim, W. M., Yeager, S. G., ... Yamazaki, D. (2018, oct). JRA-55 based surface dataset for driving ocean–sea-ice models (JRA55-do). *Ocean Modelling*, *130*, 79–139. doi: 10.1016/j.ocemod.2018.07.002

Voldoire, A. (2020). *Cnrm-cerfacs cnrm-cm6-1 model output prepared for cmip6 omip omip2.* Earth System Grid Federation. Retrieved from https://www.wdc-climate.de/ui/cmip6?input=CMIP6.OMIP.CNRM-CERFACS.CNRM-CM6-1.omip2 doi: 10

.22033/ESGF/CMIP6.10345

Table S1. Eddy dissipation coefficient λ relative errors and uncertainties computed from the NEMO-OMIP2 simulation outputs. MAE, RMSE and δ stand for the mean absolute error, root mean squared error and mean bias, respectively.

Error source	MAE	RMSE	δ
Eddy energy balance	0.0018	0.0028	0.0019
Time average	0.0017	0.0026	0.0020
Total	0.0035	0.0046	0.0038

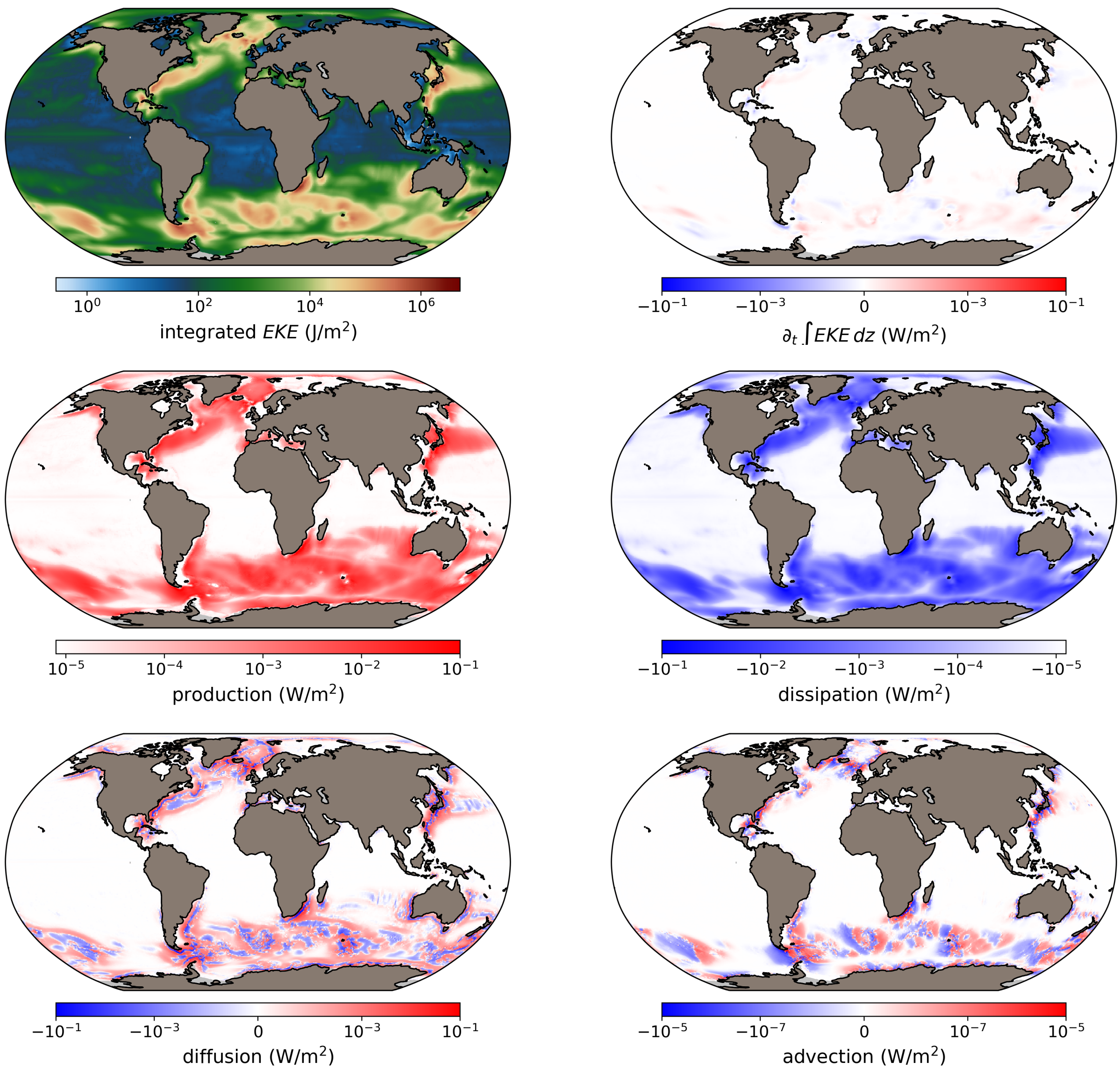

Figure S1. Global maps of eddy energy and the different trends of Equation 1 averaged over the 1995-2017 period of the NEMO-OMIP2 simulation. Since the model uses zero eddy energy background, very weak levels of EKE are found at low latitudes. Colorbars are chosen to be directly comparable except for the advection term which is at least 4 orders of magnitude smaller than other trends. All colorbars also use symmetric logarithmic scales. To convert the units into J and W, a reference density value of $\rho_0 = 1026$ kg/m^3 is used.

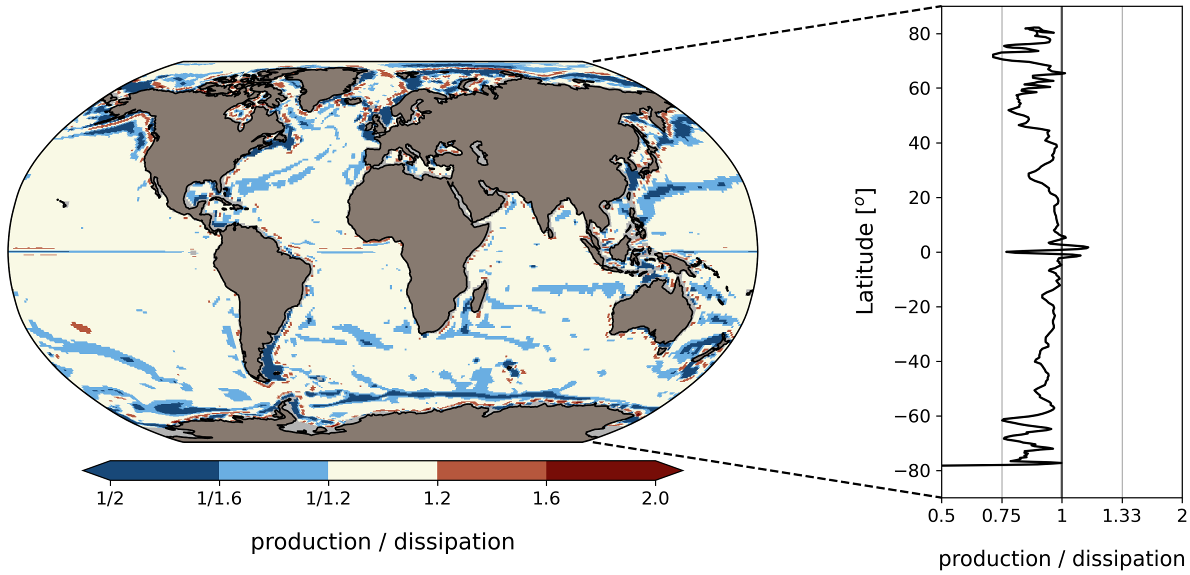

Figure S2. Ratio between baroclinic eddy energy production and linear dissipation in the NEMO-OMIP2 simulation using a parameterized eddy energy budget. Its zonal average is displayed on the right. A geometric scale is chosen for the colorbar to retain proportion both upward and downard unity while a spatial shapiro filter was also used to reduce the horizontal noise.

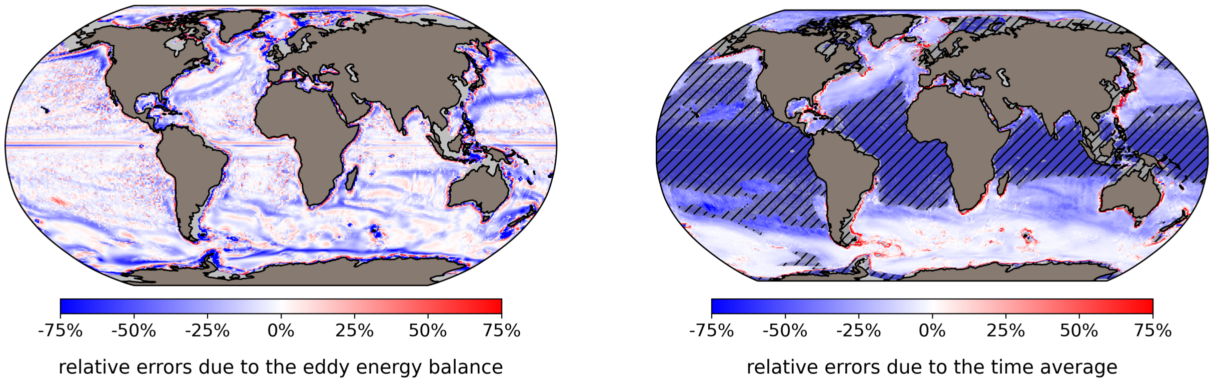

Figure S3. Relative errors due to the eddy energy balance assumption (left) and the time averaging approximation (right) from the NEMO-OMIP2 model outputs averaged from 1995 to 2017. The hatched area covers the ocean cells where the eddy induced transport coefficient κ_{gm} is capped in the GEOMETRIC implementation (see Mak et al. (2022) for details) and therefore the production term is not proportional to the eddy energy. Thus, these cells are not included in the time average error quantification.

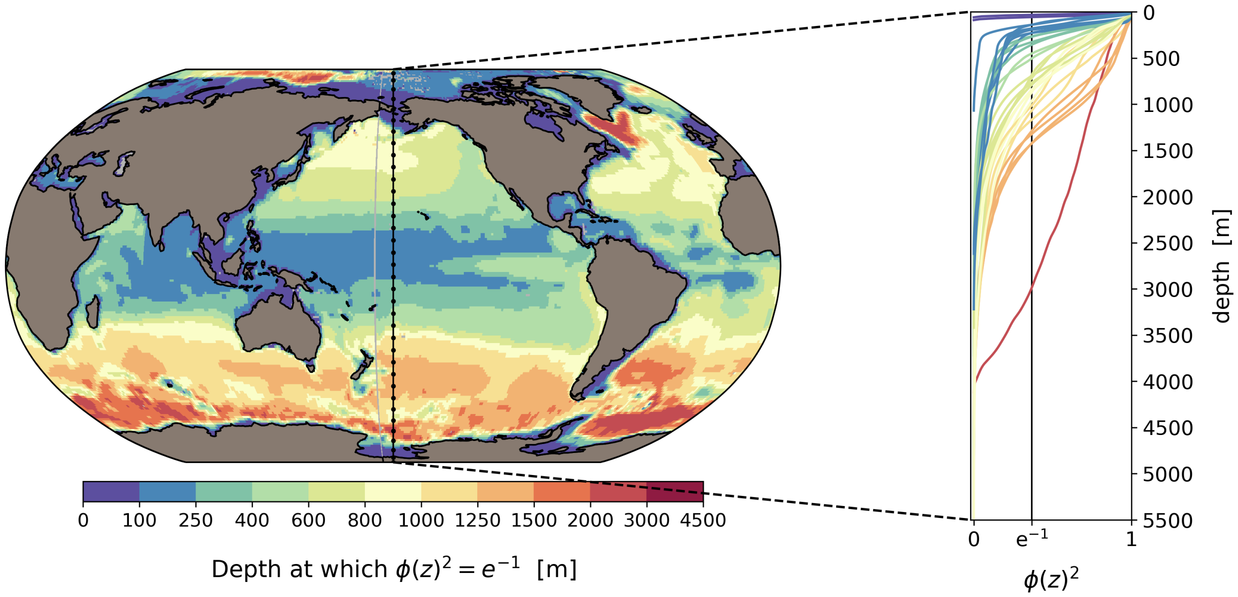

Figure S4. The e-folding depth for the EKE corresponding to the depth where $\phi(z)^2 = e^{-1}$. The map (left) represents the strenght of the EKE decrease with depth while the plot (right) shows profiles along the 171.5°W transect to illustrate the effect of the structure function on the depth integrated EKE.